CRCLEME

Cooperative Research Centre for
Landscape Environments
and Mineral Exploration

CSIRO
EXPLORATION
AND MINING

OPEN FILE
REPORT
SERIES

CHARACTERISTICS OF GOLD DISTRIBUTION AND HYDROGEOCHEMISTRY AT THE CAROSUE DAM GOLD PROSPECT, WESTERN AUSTRALIA

D.J. Gray, N.B. Sergeev and C.G. Porto

CRC LEME OPEN FILE REPORT 217

June 2007

CRCLEME

(CRC LEME Restricted Report 121R / E&M Report 664R, 2000,
2nd Impression 2007)

CHARACTERISTICS OF GOLD DISTRIBUTION AND HYDROGEOCHEMISTRY AT THE CAROSUE DAM GOLD PROSPECT, WESTERN AUSTRALIA

D.J. Gray, N.B. Sergeev and C.G. Porto

CRC LEME OPEN FILE REPORT 217

June 2007

(CRC LEME Restricted Report 121R / E&M Report 664R, 2000,
2nd Impression, 2007)

Headquarters: CRC LEME c/o CSIRO Exploration and Mining, PO Box 1130, Bentley WA 6102, Australia

The CRC LEME - AMIRA Project 504 **"SUPERGENE MOBILIZATION OF GOLD IN THE YILGARN CRATON"** was carried out over the period 1998 to 2001. Twelve reports resulted from this collaborative project.

CRC LEME acknowledges the support of the Australian Mineral Industries Research Association (AMIRA), and the major contribution of researchers from CSIRO Exploration and Mining.

Although the confidentiality periods of the research reports have expired, the last in July 2002, they have not been made public until now. In line with CRC LEME technology transfer goals, re-releasing the reports through the **CRC LEME Open File Report (OFR) Series** is seen as an appropriate means of making available the results of the research and the authors' interpretations. It is hoped that the reports will provide a source for reference and be useful for teaching.

OFR 217 - Characteristics of gold distribution and hydrogeochemistry at the Carosue Dam prospect, Western Australia - DJ Gray, NB Sergeev and CG Porto.

OFR 218 - Gold distribution, regolith and groundwater characteristics at the Mt Joel prospect, Western Australia - CG Porto, NB Sergeev and DJ Gray.

OFR 219 - Supergene gold dispersion at the Argo and Apollo deposits, Western Australia - AF Britt and DJ Gray

OFR 220 - Geochemistry, hydrogeochemistry and mineralogy of regolith, Twin peaks and Monty Dam gold prospects, Western Australia - NB Sergeev and DJ Gray.

OFR 221 - Supergene gold dispersion in the Panglo Gold deposit, Western Australia - DJ Gray.

OFR 222 - Gold concentration in the regolith at the Mt Joel prospect, Western Australia - DJ Gray.

OFR 223 - Gold dispersion I nthe regolith at the Federal Deposit, Western Australia - NB Sergeev and DJ Gray.

OFR 224 - Supergene gold dispersion in the regolith at Cleo deposit, Western Australia - AF Britt and DJ Gray.

OFR 225 - Distribution of gold arsenic chromium and copper in the regolith at the Harmony Deposit, northern Yilgarn, Western Australia - AF Britt and DJ Gray

OFR 226 - Supergene gold dispersion in the regolith at the Kanowna Belle and Ballarat Last Chance deposits, Western Australia - DJ Gray.

OFR 227 - Supergene gold dispersion, regolith and groundwater of the Mt Holland region, Southern Cross province, Western Australia - AF Britt and DJ Gray.

OFR 228 - Supergene mobilization of gold and other elements in the Yilgarn Craton, *Western Australia* - ***FINAL REPORT*** - DJ Grey, NB Sergeev, CG Porto and AF Britt

This Open File Report 217 is a second impression (updated second printing) of CRC for Landscape **Evolution** and Mineral Exploration Restricted Report No 121R, first issued in May 2000. It has been re-printed by CRC for Landscape **Environments** and Mineral Exploration (CRC LEME).

Electronic copies of the publication in PDF format can be downloaded from the CRC LEME website: http://crcleme.org.au/Pubs/OFRSindex.html. Information on this or other CRC LEME publications can be obtained from http://crcleme.org.au
Hard copies will be retained in the Australian National Library, the J. S. Battye Library of West Australian History, and the CSIRO Library at the Australian Resources Research Centre, Kensington, Western Australia.

Reference:
Gray DJ, Sergeev NB and Porto CG, 2007. Characterisation of gold distribution and hydrogeochemistry at the Carosue Dam gold prospect, Western Australia. *CRC LEME Open File Report 217*. 45pp

Keywords: 1. Supergene gold. 2. Mobilization of gold. 3. Hydrogeochemistry. 4. Carosue Dam gold prospect -Western Australia. 5. Yilgarn Craton - Western Australia. 6. Regolith.

ISSN 1329-4768
ISBN 1 921039 62 0

Addresses and affiliations of Authors:

Dr David J Gray
CRC LEME and
CSIRO Exploration and Mining
PO Box 1130
Bentley WA 6102

Dr Nikita B Sergeev
formerly CRC LEME

Dr Claudio G Porto
formerly CRC LEME, now
Cidade Universitaria
Rio de Janeiro
Brazil.

Published by: CRC LEME, c/o CSIRO Exploration and Mining, PO Box 1130, Bentley, Western Australia 6102

PREFACE

The CRC LEME-AMIRA Project 504 *Supergene mobilization of gold and other elements in the Yilgarn Craton* has, as its principal objective, determination of the mechanisms of supergene/secondary depletion, enrichment and dispersion of Au and other elements, so as to improve selection of drilling targets and further optimize interpretation of geochemical data. For this goal, it is important to develop methods for recognition and understanding of any mobilization of Au and potential pathfinder elements. This report summarizes the investigations undertaken at Carosue Dam by CRCLEME as part of AMIRA P504.

The Carosue Dam Prospect, south of Lake Rebecca, is one of three Au prospects being investigated in the Mulgabbie area, the other two sites being Twin Peaks and Monty Dam, which are within Goldfields Exploration tenements. All three sites are located within felsic rocks, with varied regolith and geomorphological environments and differing mineralization styles. In particular, there are changes in thickness of alluvial cover from less than one metre to greater than 80 m. For these reasons, this area is valuable for the enhancement of our knowledge of Au and pathfinder element dispersion during weathering of felsic rocks, and of the influence of geomorphological environment on these processes. This report gives results on the 3D distribution of Au, Au concentration calculations, Au grain investigations and hydrogeochemistry at Carosue Dam.

D.J. Gray,
Project Leader.
May, 2000

ABSTRACT

Gold mineralization at Carosue Dam occurs in felsic rocks, which are now intensely weathered. The whole area has very low relief, with an *in situ* regolith of ferruginous material (0 - 30 m), generally truncated to mottled zone, and saprolite (10 - 96 m). The saprolite is strongly depleted in Au to 30 m below surface, approximating to the base of the strongly oxidised zone. There is no secondary Au enrichment halo. There is 5 - 20 m of transported cover (colluvium-alluvium, lacustrine clays and quartz sands), including 1 - 6 m of calcrete at surface, overlying *in situ* regolith. As elsewhere in the southern Yilgarn Craton, the calcrete is highly enriched in Au, though with the Au enrichment translocated several hundred metres to the south, relative to the underlying mineralization. The northern extent of the mineralized zone has a strongly truncated laterite profile, thick transported cover and reduced Au expression at surface. For the southern part of the mineralized zone there is a near-complete residual laterite profile and less than 10 m of transported cover. At the surface, Au has been dispersed chemically and/or physically to the south, causing the observed separation between buried mineralization and surface expression in the calcrete. The surface Au distribution is less statistically skewed than at depth, indicating significant redistribution and homogenisation at the surface. Gold grain studies suggest that much of this surface mobility is due to physical transport of residual primary Au

Groundwaters at Carosue Dam are saline to hypersaline (2.5 - 11.6% TDS), and acid (pH 3.2 - 6.0), except for a single neutral (pH 7.1) sample in the SW of the study area. These ranges are similar to groundwaters at Kalgoorlie, though are less (by 2 - 3 times) saline. The Carosue Dam groundwaters are significantly K-depleted, probably due to alunite precipitation under acid conditions. However, though many of the minor elements are enriched, due to the acid conditions, the enhancement is significantly less than for acid and saline Kalgoorlie groundwaters in contact with weathered mafic and ultramafic rocks. This suggests that groundwaters in contact with weathered felsic rocks are likely to have lower hydrogeochemical signatures, when pH effects are taken into account. Because of the strong salinity and acidity control, very few elements give hydrogeochemical signatures useful for exploration. The best (though patchy) correlation with mineralization was for dissolved Au. Groundwaters at Carosue Dam are ideal for Au dissolution as the chloride ($AuCl_2^-$) or iodide (AuI_2^-) complexes. The groundwaters range from moderately to highly oxidising: two of the groundwaters have Eh values high enough to allow dissolution of > 2 µg/L Au, with another three groundwaters able to dissolve > 0.2 µg/L Au. As a consequence, dissolved Au concentrations are, unlike other minor elements, as high as, if not higher than, other sites on the Yilgarn.

TABLE OF CONTENTS

1. SITE CHARACTERISTICS 1

2. METHODS AND MATERIALS 2

2.1 Drill hole logging and sampling 2
2.2 3D gridding, visualisation and Au concentration calculations 2
2.3 Gold grain separation and analysis 4
2.4 Groundwater sampling and analysis 5

3. REGOLITH STRATIGRAPHY 7

3.1 Surface elevation and regolith stratigraphy, as defined by Aberfoyle logging 7
3.2 Regolith stratigraphy defined by CRC LEME logging and comparison with Aberfoyle and Pacmin results 10

4. GOLD GEOCHEMISTRY / 3D MODELLING 14

4.1 Results for the 3125N Traverse 14
4.2 Raw data Au concentration calculations 14
4.3 MVS calculations of Au concentrations 15
4.4 Visualisations of Au concentration 19

5. CHARACTERISTICS OF PARTICULATE GOLD AT CAROSUE DAM 24

5.1 Introduction 24
5.2 Characteristics of gold grains 24
5.3 Primary mineralization 24
5.4 Gold dispersion halo within saprolite 25
5.5 Subsurface anomaly 25
5.6 Discussion 26

6. HYDROGEOCHEMISTRY 27

6.1 Introduction 27
6.2 Compilation of results and comparison with other sites 27
6.3 Acidity and oxidation potential 28
6.4 Salinity effects and major element hydrogeochemistry 29
6.5 Minor element hydrogeochemistry 32
6.6 Gold chemistry 34
6.7 Mapping of the groundwater data 34

7. SUMMARY AND CONCLUSIONS 36

APPENDICES

APPENDIX 1: CONTENTS OF ENCLOSED CD

APPENDIX 2: ELEMENT/ION CONCENTRATIONS FOR GROUNDWATERS

APPENDIX 3: SATURATION INDICES FOR GROUNDWATERS

APPENDIX 4: ELEMENT/ION DISTRIBUTION MAPS FOR GROUNDWATERS

LIST OF FIGURES

FIGURE 1: DIAGRAMMATIC REPRESENTATION OF METHOD OF CALCULATING AU CONCENTRATION FROM SLICES DEFINED FOR THE UPPER SURFACE AND FOR THE UNCONFORMITY. 3
FIGURE 2: CALCULATED (A) REGOLITH RELIABILITY, (B) UNFILTERED AU CONCENTRATION AND (C) FILTERED (> 60% RELIABILITY) AU CONCENTRATION COLOUR CODED TO RELIABILITY. 4
FIGURE 3: GROUNDWATER SAMPLE POSITIONS AND SAMPLING DEPTHS, WITH CONTOURED AU DATA FOR ALL ANALYSED REGOLITH SAMPLES BETWEEN 314 AND 331 MRL, CAROSUE DAM. 5
FIGURE 4: SURFACE TOPOGRAPHY (IN MRL) AT CAROSUE DAM, WITH GREY FILL REPRESENTING AREAS WITH GREATER THAN 200 PPB AU FOR THE 314 – 331 MRL INTERVAL. 7
FIGURE 5: OBLIQUE VIEW FROM SW OF EXPLODED BLOCK MODEL, CAROSUE DAM, ILLUSTRATING REGOLITH STRATIGRAPHY. 8
FIGURE 6: CALCULATED THICKNESS OF ALLUVIUM FOR CAROSUE DAM. BLACK LINES REPRESENT 200 PPB AU CONTOUR FOR 314 – 331 M RL INTERVAL. 9
FIGURE 7: CALCULATED THICKNESS OF FERRUGINOUS ZONE (SECTION 2.1) FOR CAROSUE DAM. 9
FIGURE 8: CRC LEME AND ABERFOYLE LOGGING INFORMATION FOR DRILL HOLE PD 16 11
FIGURE 9: CRC LEME AND ABERFOYLE LOGGING INFORMATION FOR DRILL HOLE PD 50 12
FIGURE 10: SUMMARIZED CRC LEME AND ABERFOYLE LOGGING INFORMATION FOR CAROSUE DAM SECTION 3125N13
FIGURE 11: GOLD GEOCHEMISTRY FOR CAROSUE DAM SECTION 3125N 14
FIGURE 12: MEAN AU GRADES (RAW DATA) VS. MRL DEPTH. 15
FIGURE 13: GEOMETRIC MEAN AU GRADE (RAW DATA) VS. MRL DEPTH 15
FIGURE 14: THICKNESSES OF EACH REGOLITH LAYER, CAROSUE DAM. 16
FIGURE 15: MEAN AU FOR EACH REGOLITH LAYER, CAROSUE DAM. 16
FIGURE 16: THICKNESSES OF REGOLITH LAYERS OPTIMISED FOR AU CONCENTRATION DISCRIMINATION, CAROSUE DAM. 16
FIGURE 17: MEAN AU OF REGOLITH LAYERS OPTIMISED FOR AU CONCENTRATION DISCRIMINATION, CAROSUE DAM 16
FIGURE 18: MEAN AU VS. DISTANCE FROM THE WEATHERING FRONT, CAROSUE DAM. 17
FIGURE 19: MEAN AU VS. DISTANCE FROM THE WEAKLY TO MODERATELY OXIDISED TRANSITION, CAROSUE DAM. 17
FIGURE 20: MEAN AU VS. DISTANCE FROM THE MODERATELY TO STRONGLY OXIDISED TRANSITION, CAROSUE DAM. 18
FIGURE 21: MEAN AU VS. DISTANCE FROM THE PEDOPLASMATION FRONT (BASE OF FERRUGINOUS ZONE), CAROSUE DAM.18
FIGURE 22: MEAN AU VS. DISTANCE FROM THE UNCONFORMITY, CAROSUE DAM. 18
FIGURE 23: MEAN AU VS. DISTANCE FROM THE BASE OF CALCRETE, CAROSUE DAM. 18
FIGURE 24: MEAN AU VS. DEPTH FROM SURFACE FOR TRANSPORTED OVERBURDEN, CAROSUE DAM. 19
FIGURE 25: MEAN AU VS. ELEVATION FOR CAROSUE DAM. 19
FIGURE 26: CONTOURED AU DATA AT 300 MRL (BELOW DEPLETED ZONE), CAROSUE DAM. 20
FIGURE 27: CONTOURED AU DATA AT 340 MRL (DEPLETED ZONE), CAROSUE DAM 20
FIGURE 28: CONTOURED AU DATA FOR THE REGOLITH SURFACE, CAROSUE DAM. 20
FIGURE 29: GOLD DISTRIBUTION USING A 0.05 PPM CUT-OFF, CAROSUE DAM 22
FIGURE 30: CALCULATED AU GRADE FOR 8200 ME TRAVERSE, CAROSUE DAM (2X VERTICAL EXAGGERATION) 22
FIGURE 31: POSSIBLE ORIGIN OF SURFACE AU ANOMALY AT CAROSUE DAM 23
FIGURE 32: POSITION OF AU GRAIN SAMPLING, FROM CAROSUE DAM SECTION 3125N 24
FIGURE 33: EH VS. PH FOR GROUNDWATERS FROM CAROSUE DAM AND OTHER SITES 29
FIGURE 34: PH VS. TDS FOR GROUNDWATERS FROM CAROSUE DAM AND OTHER SITES 30
FIGURE 35: SCANDIUM VS. PH FOR CAROSUE DAM AND OTHER WESTERN AUSTRALIAN GROUNDWATERS. 32
FIGURE 36: DISSOLVED AU CONCENTRATION VS. EH FOR CAROSUE DAM AND OTHER WESTERN AUSTRALIAN GROUNDWATERS 34
FIGURE 37: DISSOLVED AU DISTRIBUTION AT CAROSUE DAM 35

LIST OF TABLES

TABLE 1: SUMMARY OF THE REGOLITH STRATIGRAPHY TERMS USED IN THIS REPORT, WITH APPROXIMATE EQUIVALENCIES BETWEEN LOGGING SYSTEMS. 10
TABLE 2: GOLD CONCENTRATION OF THE BULK SAMPLES, WITH SAMPLE NUMBERS AS USED *IN FIGURE 32* 24
TABLE 3: COMPARATIVE CHARACTERISTICS OF THE PRIMARY AND SUPERGENE AU, CAROSUE DAM 25
TABLE 4: SI VALUES FOR THE CAROSUE DAM GROUNDWATERS, FOR A NUMBER OF RELEVANT SOLID PHASES 31
TABLE 5: MEDIAN MINOR ELEMENT COMPOSITIONS OF GROUNDWATERS. 33

1. SITE CHARACTERISTICS

This Section is based on information supplied by H.W. Rowlands, formerly of Aberfoyle Resources Limited. The Carosue Dam gold deposit is located approximately 110 km north east of Kalgoorlie and 6 km west of the Mulgabbie Mining Centre, at 30°10'S, 122°22'E. The deposit is one of several deposits and prospects discovered within the Khartoum E28/372 licence, which is owned by Aberfoyle Resources Limited. An inferred resource of 5.5 Mt @ 3 g/t Au was reported for the Carosue Dam deposit in September 1997. Total resources for the Khartoum licence were 10.8 Mt @ 2.9 g/t Au as at June 1998, from the Carosue Dam, Whirling Dervish and Luvironza deposits.

The project area lies in the eastern part of the Norseman-Wiluna greenstone belt in the Eastern Goldfields Province of the Archaean Craton. The Carosue Dam deposit lies within the Gundockerta Formation (acid volcanic-clastic association IV), on the western limb of the regional Yilgangi Syncline. The lithologies at Carosue Dam comprise andesite, trachyte and rhyodacite, intermediate-acid volcanoclastic sandstones and crystal tuffs, shale and siltstone. The rock units strike approximately northwest with moderate (60°) northeasterly dips. The whole area is generally flat and deeply weathered. The deposit is concealed by 8 - 30 m of transported cover, comprising colluvium-alluvium, lacustrine clay and quartz sand. Beneath the transported cover, strongly leached Archaean saprolite occurs to 30 - 60 m depth.

Gold mineralization is confined to the volcanoclastic sandstones and lesser trachytic volcanics and/or dykes, and is associated with albite, K-feldspar, silica, hematite, carbonate, and pyrite alteration.

Mineralization in the fresh rock occurs in multiple lodes, with two orientations:

I. sub-parallel to lithological contacts, striking northwest and dipping moderately to the northeast, and

II. west-northwest striking and dipping shallowly to the northeast with a gentle northerly plunge (silica-albite-pyrite rich and of higher gold grade).

Mineralization is structurally confined to faults, shear zones and lithological contacts. To the west mineralization is cut-off by a north trending fault, with shales and siltstones (distal volcanoclastics) located to the west. To the southeast, mineralization is truncated by a schistose volcanoclastic unit (Yilgangi shear zone). Late-stage post mineralization east-west trending faults disrupt the northwest striking lithologies and associated mineralization; the northern blocks are upthrown.

The regolith is more than 80 m thick and transported overburden is present, being up to 20 m in the study area. Further south of the study area, where the residual profile is overlain by palaeochannels, the thickness of transported overburden increases to greater than 80 m.

2. METHODS AND MATERIALS

2.1 Drill hole logging and sampling

An EW section across the mineralized zone at 3125 mN was selected for detailed work on the basis of geological information and condition of drill spoils. Drill holes logged were seven RC holes to the west, with six shallower RAB holes to the east. Logging was based mostly on bulk colour of the samples, guided by the Munsell colour charts, and the nature of coarse fragments obtained by wet sieving of approximately 300 g of each sample. Selected bulk samples were collected for Au grain studies (Section 2.3).

2.2 3D gridding, visualisation and Au concentration calculations

The regolith stratigraphy and geochemistry of the Carosue Dam Au prospect were studied using the 3D visualisation program MVS (Mining Visualisation System; © C Tech Development Corporation, with geochemical and logging information initially provided by Aberfoyle Resources, with additional drilling data as provided by Pacmin Mining Corporation. Conclusions are based on the expanded Au database from Pacmin with the logging as provided by Aberfoyle. This logging showed major spatial and temporal variations, presumably due to changes in staff and different emphases on regolith units. After careful checking and filtering, seven separate surfaces were delineated:

(i) natural surface;
(ii) base of carbonate horizon;
(iii) unconformity at base of transported cover;
(iv) pedoplasmation front (top of saprolite);
(v) strongly to moderately oxidised transition;
(vi) moderately to weakly oxidised transition;
(vii) base of weathering.

The materials between the unconformity and pedoplasmation front can include duricrust, lateritic residuum, mottled zone and Fe-depleted material, though the regolith is commonly depleted to mottled zone. For the sake of simplicity all these materials are denoted as the ferruginous zone in the text.

Regolith horizons were gridded, "point" anomalies removed from the input data, and the data re-gridded. Although this filtering has the potential to bias the data, it was considered necessary to give coherent weathering horizons. For pictorial presentations, the data were pre-processed by logarithmic transform (base 10) of Au concentrations before gridding (Porto *et al*. 1999). Although this can affect the gridded magnitude of the main mineralization pattern, it enhances the detail of the subtle supergene redistributions. For Au grade calculations (see below), untransformed data was used. Surface geochemical data were commonly collected as 4 m composites, which can lead to deeper and weaker surface anomalies (*e.g.*, a horizon that is 1 m at 0.5 ppm, then 3 m at 0.1 ppm, will effectively be 4 m at 0.2 ppm where 4 m composites are used).

Stratigraphy was gridded with the KRIG_3D_GEOLOGY module within MVS. The kriging domain was confined to the region defined by the sample locations (convex hull), with the convex hull boundary offset to 0.05, maximum number of samples points set to 80, and other settings at default. Geochemistry was then kriged in relation to these surfaces, using the KRIG_3D module. The maximum number of data points (within the specified reach) that will be considered for the parameter estimation at a model node were set to 180, horizontal/vertical anisotropy set at 2.5 (data points in a horizontal direction away from a model node influence the kriged value at that node 2.5 times more than data points an equal distance away in a vertical direction), rectilinear offset parameter at 0.05, post-processing at maximum 2 ppm Au, and all other settings at default. The grid size used was X:Y:Z - 10 m:10 m:3 m.

Gold concentrations were calculated with untransformed data, using the VOLUME_AND_MASS module. No attempt was made to model different densities for different units. As the Au grade data is as mass/mass rather than mass/volume, uniform density has only a minor influence on most calculations. The calculated concentrations do not compensate for leaching of mobile constituents: if half of the minerals have dissolved and been leached then Au grade will double because of residual concentration.

In addition, (using the ISOVOLUME module) Au concentrations can be calculated for slices defined either by elevation (e.g., 390-393 m RL) or distance from a regolith boundary (*e.g.*, 3-6 m above the unconformity). Most analyses were done using 3 m vertical spacings. For some critical transitions where Au concentrations appeared to change more abruptly than could be accurately determined using a 3 m vertical spacing, data was re-gridded and concentrations calculated using a 0.5 m vertical spacing.

Figure 1 illustrates nominal 3 m slices taken downwards from the unconformity, which become truncated downwards at the base of weathering, as the analysis is set up not to include the next regolith horizon. While this method may be arithmetically correct, it can lead to over- or under-estimations of concentrations as the slices get further from the reference transition (in this case the unconformity). This is because, ultimately, the slice being analyzed is not complete, again illustrated in Figure 1 as the slices becoming more and more truncated by the base of weathering. Note that this is not a problem in calculation accuracy, but in the actual geometry of the study area. This can be expressed as a reliability factor, which is the mass of the slice divided by the mass of an untruncated slice (Figure 1). A reliability index of 85% indicates that the slice is 15% truncated.

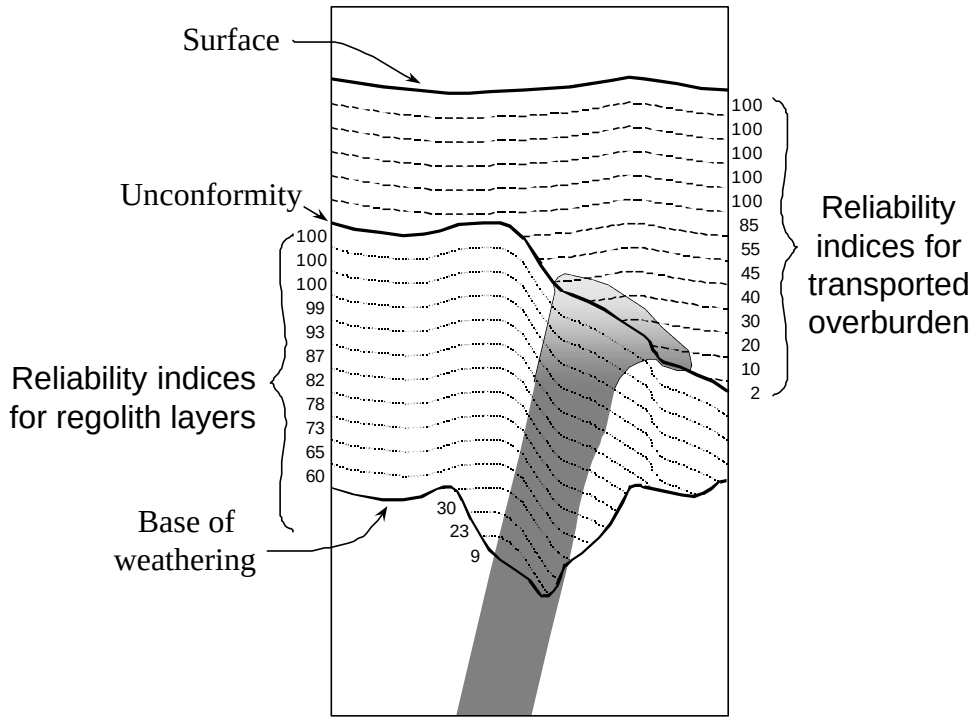

Figure 1: Diagrammatic representation of method of calculating Au concentration from slices defined for the upper surface and for the unconformity.

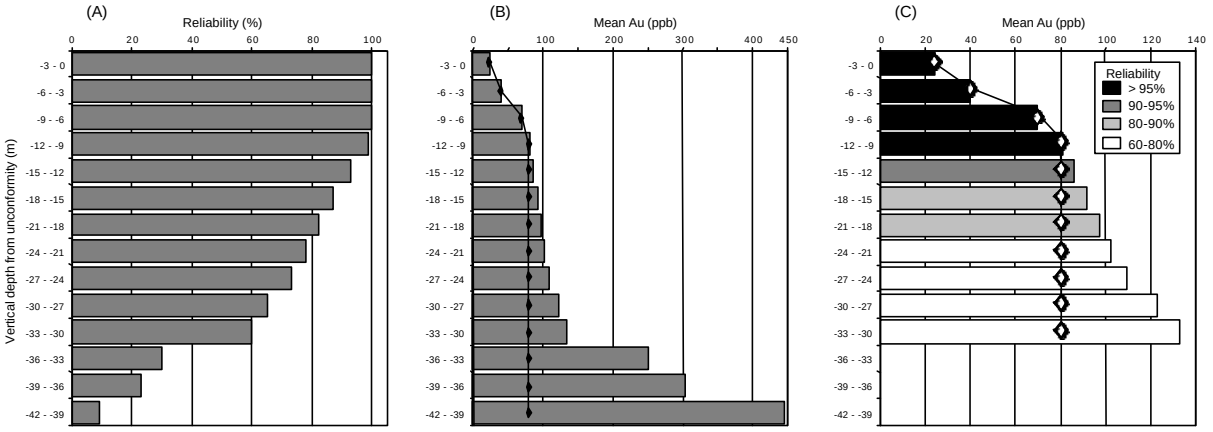

Figure 2: Calculated (A) regolith reliability, (B) unfiltered Au concentration and (C) filtered (> 60% reliability) Au concentration colour coded to reliability. Diamonds represent expected Au concentration. Data based on situation represented in Figure 1.

As the reliability index decreases, significant errors can occur. Figure 2 shows the results of Au concentration measurement for each slice from the unconformity. Though the deeper slices are truncated (Figure 2A), they can still contain mineralized material, as in this example (Figure 1). Thus, a similar mass of Au is being divided by smaller and smaller amounts of regolith, which leads to anomalous Au concentrations (Figure 2B). In this example, the results indicate that the deepest slice has up to 440 ppb Au even though the "real" Au content is invariant at 80 ppb, except for the leached zone at the top of the *in situ* regolith.

When all the slices with reliability indices less than 60% are removed, the remaining results can be coded for reliability (Figure 2C). A much clearer picture of the Au trends is observed, illustrating the depletion at the unconformity. Note that this example is for the maximum possible overestimation of Au grade (the maximum overestimation = 100 ÷ reliability: *e.g.*, when reliability is 60%, maximum overestimation is 1.67; when reliability is 90%, maximum overestimation is 1.11). In other cases underestimation can occur for low reliability samples (due to truncated intersection with mineralization). In summary, those samples with reliabilities less than 80% are suspect (but can still be valuable if treated with caution), whereas those with reliability less than 60% should generally not be used.

2.3 Gold grain separation and analysis

Ten bulk samples were collected for separation of Au particles. Samples were dried, split and 4.0 - 4.5 kg subsamples washed with a non-ionic surfactant (0.01% Triton X-100). Separation was performed on a Haultain Superpanner, which is essentially a mechanised version of the prospectors pan. The small, gram-size heavy concentrate was transferred into the trough of a micropanner, to separate Au grains. Gold particles were recovered under a binocular microscope by sticky needle and deposited on the slide on two-sided adhesive tape.

The morphology and size of the Au grains were examined using an optical microscope. Following this, the morphologies of the selected particles were examined by scanning electron microprobe (SEM). Their Ag content and the composition of neighbouring minerals were determined semi-quantitatively (limited by surface effects of the unpolished grains) using an energy dispersive detector. The SEM study was done in backscattered electron mode, using a Philips XL40 instrument fitted with an environmental sample chamber. This permitted examination of samples without a conductive coating.

Selected Au grains were analysed quantitatively by electron microprobe using a Cameca SX-50 instrument operated at 30 kV and 450 nA. Polished mounts were prepared by totally embedding and

carefully polishing down to expose the grains. Long count times (100 sec) were used to reduce detection limits. Native Au was analysed for Au, Ag, Cu, Fe, Si and Pd.

2.4 Groundwater sampling and analysis

Twenty one groundwater samples were collected on site by bailer in December 1997, of which 18 (one sampled from 281 mRL and the others from 306 to 327 mRL) were deemed uncontaminated and suitable for analysis (Figure 3). Included in this Figure is the contoured Au data for the regolith at the depth range of most groundwater samples.

Waters were analysed for pH, temperature, conductivity and oxidation potential (Eh), at the time of sampling. A 125 mL aliquot was collected in a polyethylene bottle (with overfilling to remove all air) for HCO_3^- analysis by alkalinity titration in the laboratory. About 1.5 L of water was filtered on site through a 0.2 µm membrane filter. About 100 mL of the filtered solution was acidified [0.1 mL 15 moles/litre (M) nitric acid], and analysed for:

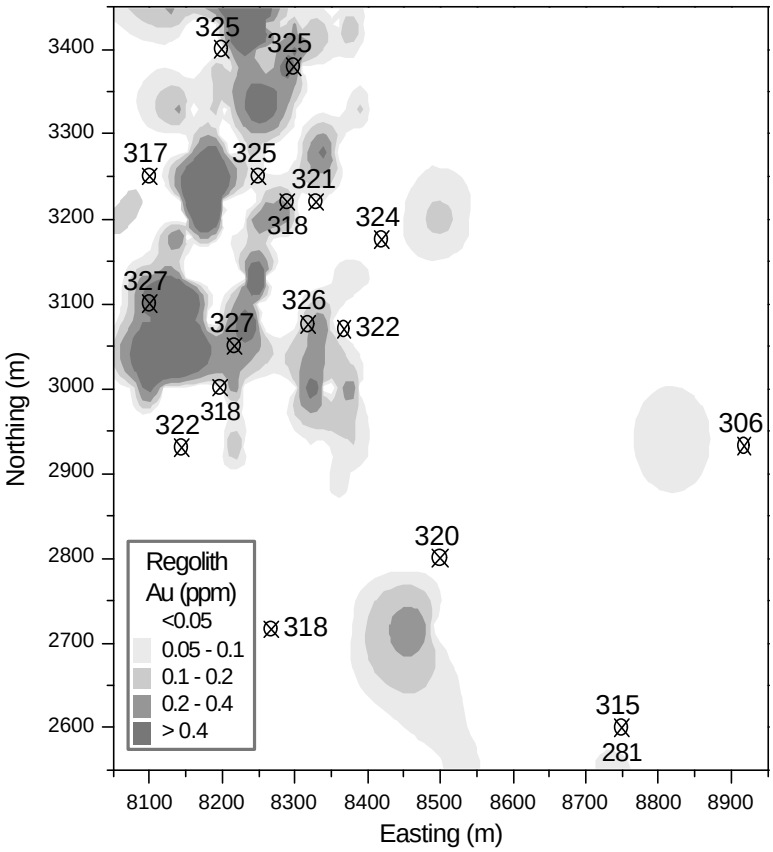

Figure 3: Groundwater sample positions and sampling depths, with contoured Au data for all analysed regolith samples between 314 and 331 mRL, Carosue Dam.

(i) Al, B, Ba, Be, Ca, Cd, Co, Cr, Cu, Fe, K, Li, Mg, Mn, Mo, Na, Ni, P/I (distinction between P and I is difficult due to spectral overlap), SO_4 (measured as S), Si, Sr, Ti, V, and Zn by Inductively Coupled Plasma - Atomic Emission Spectroscopy;
(ii) Ag, Bi, Cd, Ce, Dy, Er, Eu, Ga, Gd, Ge, Ho, La, Mo, Nd, Pb, Pr, Rb, Sb, Sc, Sm, Sn, Tb, Th Tl, Tm, U, W, Y, Yb and Zr by Inductively Coupled Plasma - Mass Spectroscopy;
(iii) total phosphate by the molybdenum blue colormetric method (Murphy and Riley, 1962);
(iv) I by subtraction of P from P/I concentration.

About 50 mL of the filtered water was collected separately, without acidification, and analysed for Cl by the Technicon Industrial method (Zall *et al*., 1956).

A one litre sub-sample of the filtered water was acidified with 1 mL 15 M HNO_3 and one gram sachet of activated carbon added. The bottle was rolled for eight days in the laboratory and the water discarded. The carbon was then analysed for Au by Instrumental Neutron Activation Analysis (INAA) at Becquerel Laboratories, Lucas Heights. The method was tested by shaking Au standards of varying concentrations, and in varying salinities, with activated carbon (Gray, unpublished data).

The solution species and degrees of mineral saturation were computed from the solution compositions using the program PHREEQE (Parkhurst *et al*., 1980; described in detail in Gray, 1990 and Gray, 1991), which determines the chemical speciation of many of the major and trace elements. To obtain highly accurate speciation data on a limited suite of the major elements (Na, K, Mg, Ca, Cl, HCO_3, SO_4, Sr and Ba), the specific ion interaction model, known as the Pitzer equations, was applied, using the program PHRQPITZ (Plummer and Parkhurst, 1990). These programs calculate the solubility indices (SI) for each water sample for various minerals. If the SI for a mineral equals zero (empirically from -0.2 to 0.2 for the major element minerals, and -1 to 1 for the minor element minerals), the water is regarded as being in equilibrium with that mineral, under the conditions specified. Where the SI is less than zero, the solution is under-saturated with respect to that mineral, so that, if present, the phase may dissolve. If the SI is greater than zero, the solution is over-saturated with respect to this mineral, which can potentially precipitate from solution. Note that this analysis only specifies possible reactions, as kinetic constraints may rule out reactions that are thermodynamically allowed. Thus, for example, waters are commonly in equilibrium with calcite, but may become over-saturated with respect to dolomite, due to the slow rate of solution equilibration and precipitation of this mineral (Drever, 1982).

These modelling determinations are important in understanding solution processes at a site. They have particular value in determining whether the spatial distribution of an element is correlated with lithology or mineralization, or whether it is related to weathering or environmental effects. Thus, if Ca distribution is controlled by equilibrium with gypsum in all samples, the spatial distribution of dissolved Ca will reflect SO_4 concentration alone and will have no direct exploration significance.

3. REGOLITH STRATIGRAPHY

3.1 Surface elevation and regolith stratigraphy, as defined by Aberfoyle logging

The Carosue Dam area slopes downwards from SW to NE (Figure 4), with the regolith stratigraphy (from Aberfoyle logging) as shown in Figure 5. There is a surface layer (generally 1 - 6 m) of carbonate-rich material, within 5 - 20 m of transported cover (Figure 6). The *in situ* regolith is composed of 0 - 30 m of ferruginous material (Figure 7), generally truncated to mottled zone, and 10 - 96 m of saprolite that is designated as strongly, moderately or weakly oxidised. The average thicknesses of each unit are:

(i) calcrete – 3 m;
(ii) carbonate-poor alluvium – 5.7 m;
(iii) ferruginous zone – 14.2 m;
(iv) strongly oxidised saprolite – 19.1 m;
(v) moderately oxidised saprolite – 15.4 m;
(vi) weakly oxidised saprolite – 15.5 m.

This site differs from the Kalgoorlie area in that the carbonate zone is significantly deeper than 1 m, though, in comparison with Safari (Bristow *et al*., 1996b), approximately 70 km N of Carosue Dam, calcification still occurs at surface. Safari is also similar to Carosue Dam in that the transported material is about 5 - 10 m thick over the deposit.

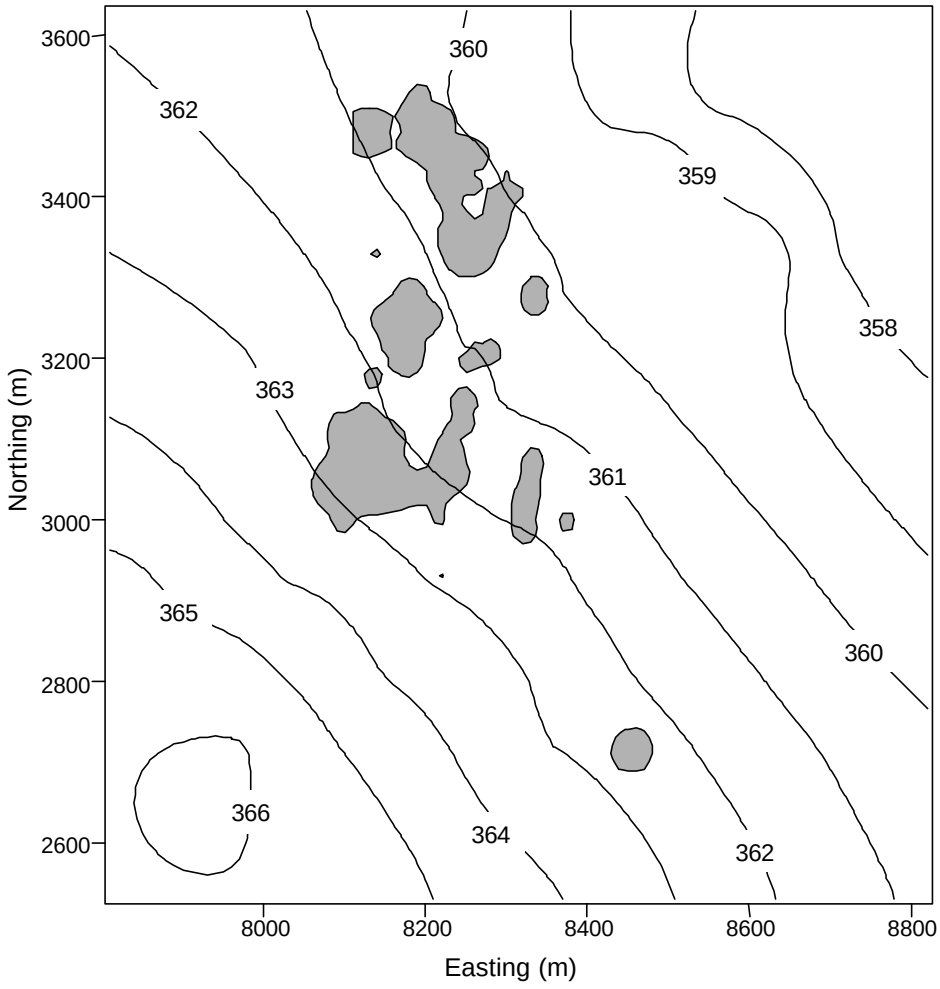

Figure 4: Surface topography (in mRL) at Carosue Dam, with grey fill representing areas with greater than 200 ppb Au for the 314 – 331 mRL interval.

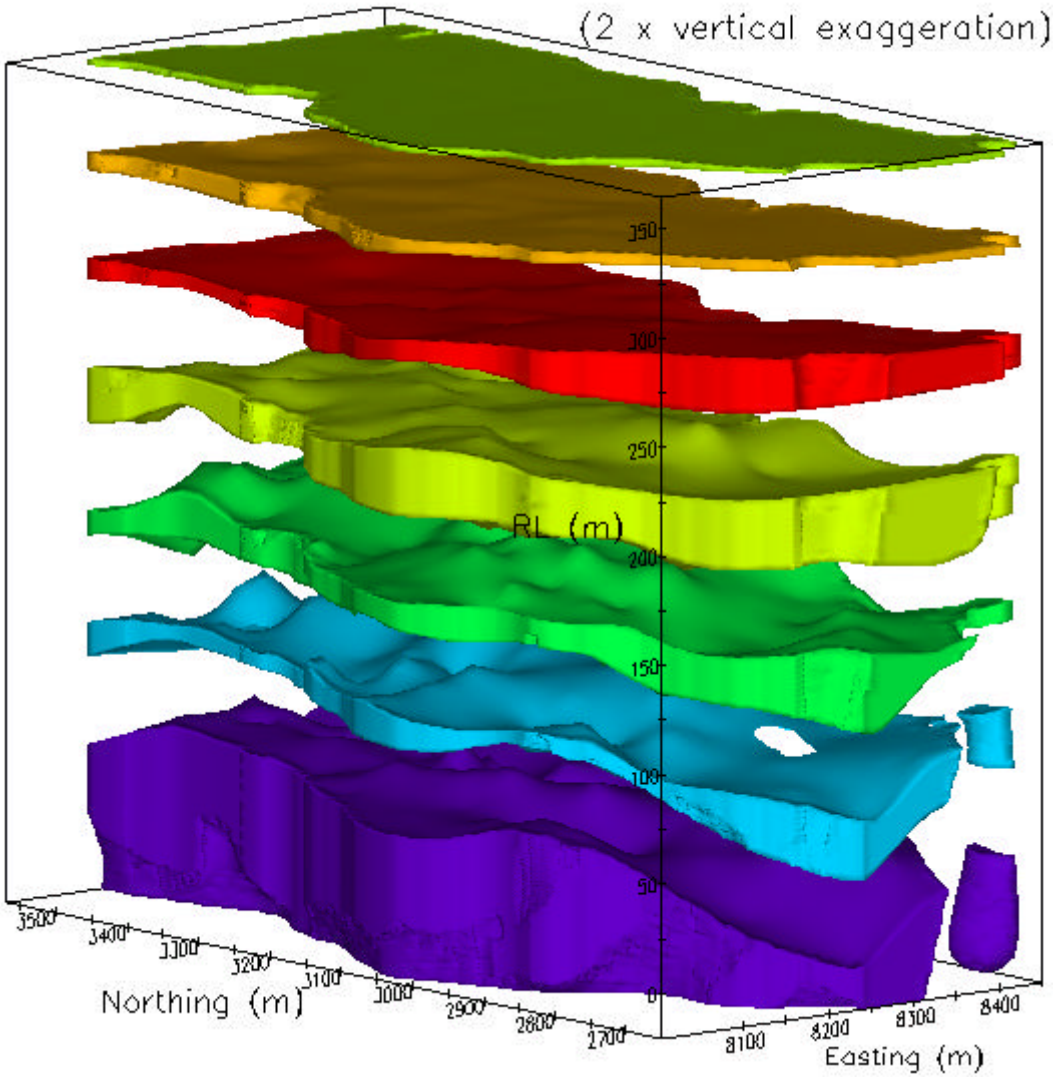

Figure 5: Oblique view from SW of exploded block model, Carosue Dam, illustrating regolith stratigraphy. Key: purple - rock, blue - weakly oxidised saprolite, green - moderately oxidised saprolite, yellow - strongly oxidised saprolite, red - ferruginous zone (Section 2.1), orange - transported cover, yellow/green - carbonate zone.

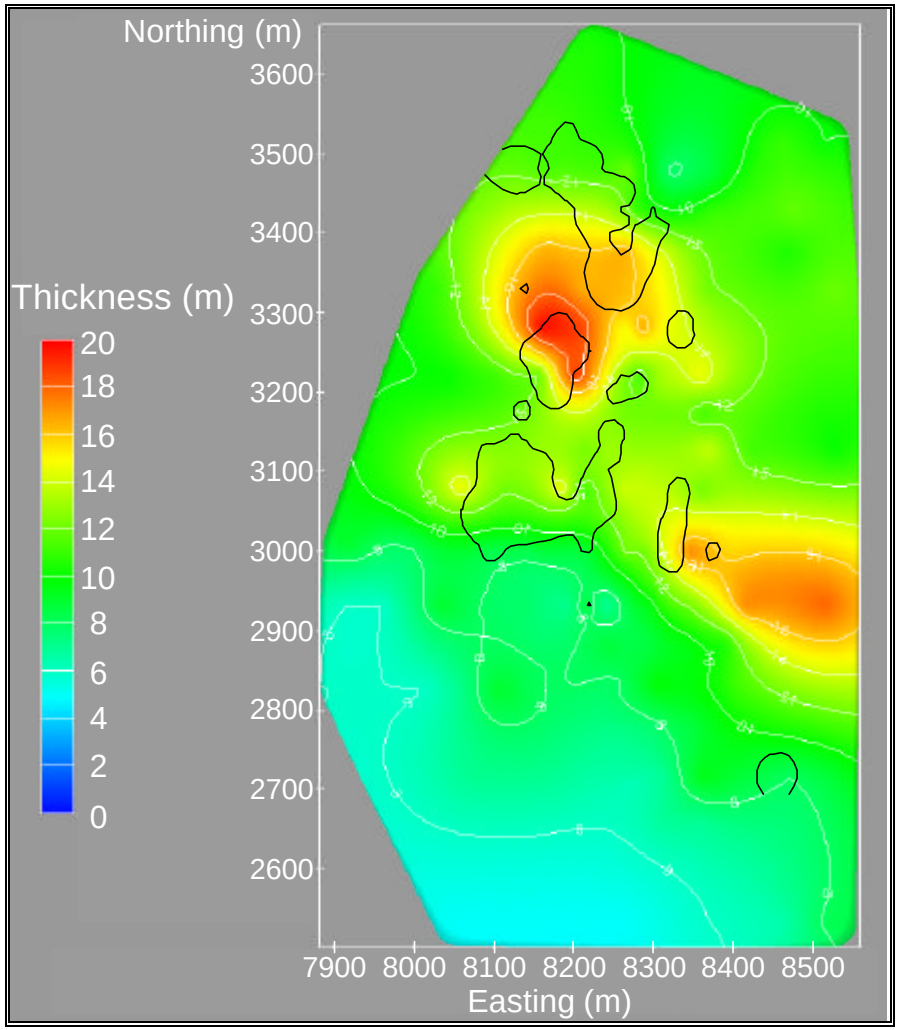

Figure 6: Calculated thickness of alluvium for Carosue Dam. Black lines represent 200 ppb Au contour for 314 – 331 m RL interval.

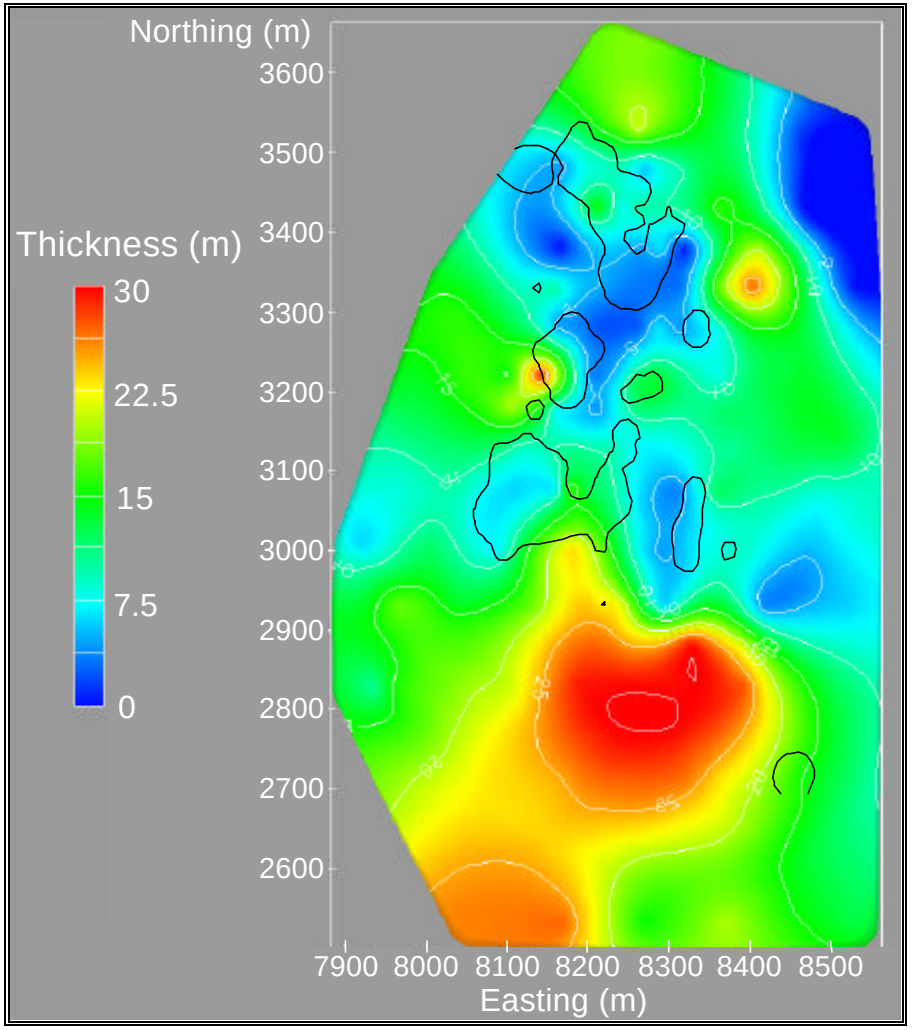

Figure 7: Calculated thickness of ferruginous zone (Section 2.1) for Carosue Dam. Black lines represent 200 ppb Au contour for 314 – 331 m RL interval.

3.2 Regolith stratigraphy defined by CRC LEME logging and comparison with Aberfoyle and Pacmin results

Further regolith information derives from CRC LEME logging of drill holes along section 3125N (Section 2.1). Sample logs for PD16 (Figure 8) and PD50 (Figure 9) are shown with CRC LEME and Aberfoyle logging, with summarized logging for the entire section shown in Figure 10.

The Base of Weathering along this section is 50 - 75 m deep. Above it, a Saprock unit has been defined based on the presence of relatively fresh rock-bearing fragments with green or greyish colours. It coincides approximately with the combined weakly and moderately oxidized zones logged by Aberfoyle. The Saprock grades up into the more creamy-coloured saprolite, which approximately correlates with the strongly oxidized zone. Intermittently, the upper saprolite becomes ferruginized. Above the saprolite are transitional material and a mottled zone, both of variable thickness, which together correlate with the Aberfoyle logged "mottled zone". However, this correlation between CRC LEME and Aberfoyle logging appears less close than for the deeper regolith zones. Additionally, because these zones are relatively thin the relative error is large. Above the mottled zone is a mixing zone, commonly characterized by red clay, between residuum and transported overburden. The alluvium consists of lateritic gravels overlain by calcrete. The transition to the transported cover is characterized by a change to red colours, magnetic Fe nodules (Figure 8 and Figure 9), and the general polymictic nature of the fragments. There is generally good agreement between the CRC LEME, Aberfoyle and Pacmin logged unconformity. Logging equivalencies are summarized in Table 1.

Table 1: Summary of the regolith stratigraphy terms used in this report, with approximate equivalencies between logging systems.

<table>
<tr><th>Aberfoyle logging</th><th>Pacmin logging</th><th>CRCLEME logging</th></tr>
<tr><td>Calcrete</td><td>Calcrete</td><td>Calcrete</td></tr>
<tr><td>Alluvium</td><td>Alluvium</td><td>Alluvium</td></tr>
<tr><td rowspan="3">Ferruginous zone</td><td>Lateritic residuum</td><td rowspan="3">Mottled zone
with some
lateritic gravels</td></tr>
<tr><td>Mottled zone</td></tr>
<tr><td>Pallid zone</td></tr>
<tr><td>Strongly oxidised</td><td>Saprolite</td><td>Saprolite</td></tr>
<tr><td>Moderately oxidised</td><td rowspan="3">Rock
⇓</td><td rowspan="2">Saprock</td></tr>
<tr><td>Weakly oxidised</td></tr>
<tr><td>Fresh</td><td>Fresh</td></tr>
</table>

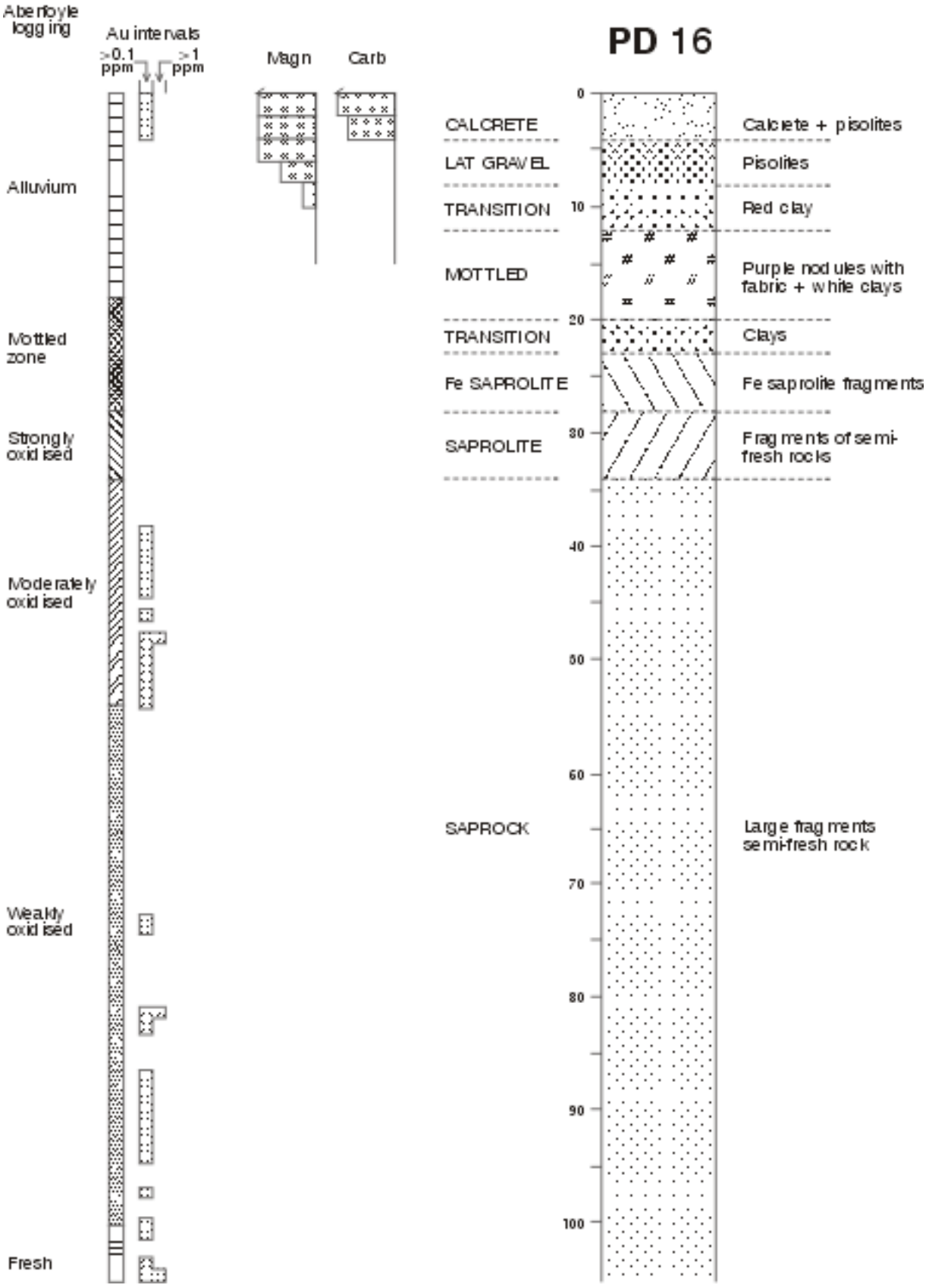

Figure 8: CRC LEME and Aberfoyle logging information for Drill hole PD 16

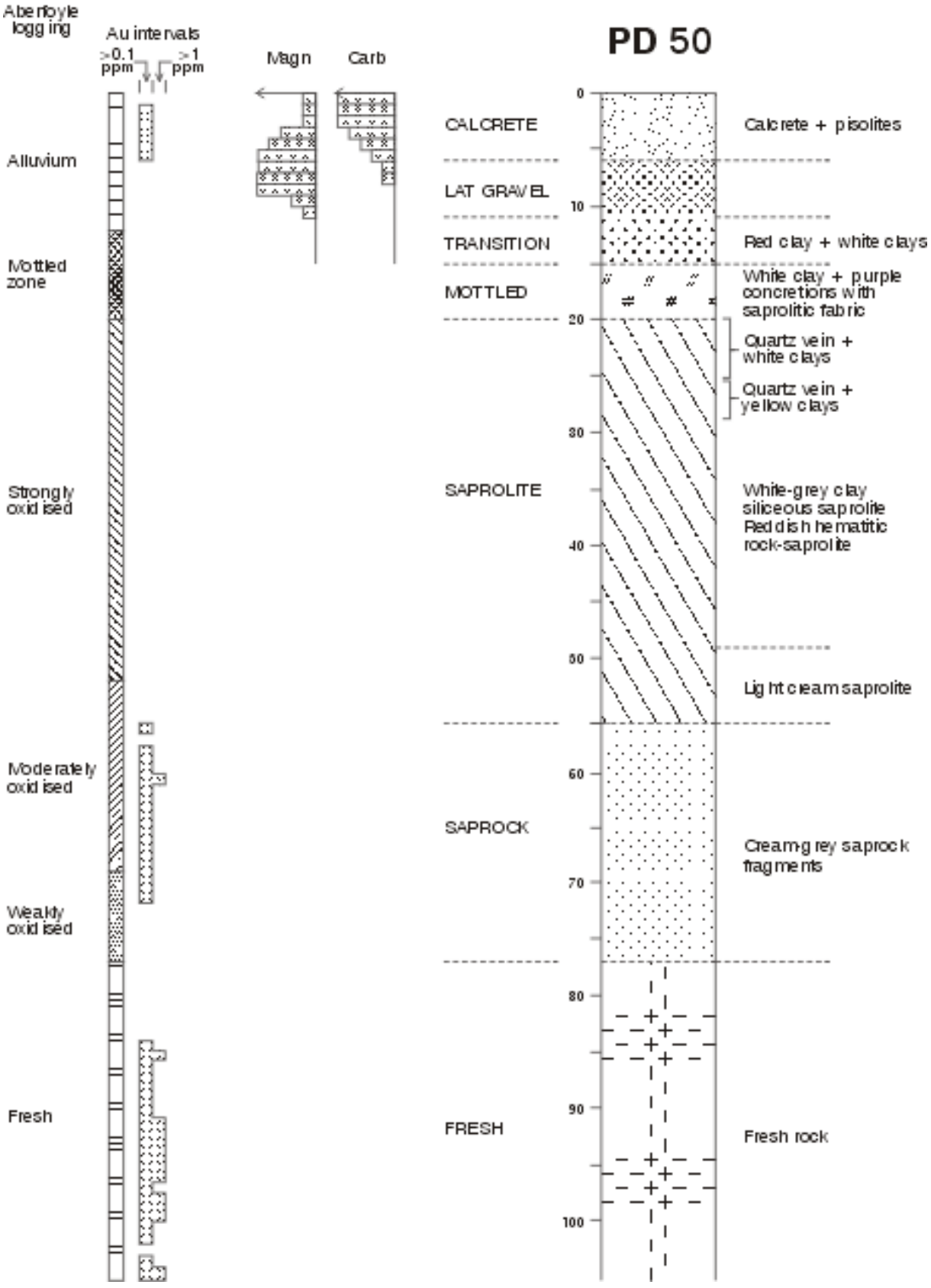

Figure 9: CRC LEME and Aberfoyle logging information for Drill hole PD 50

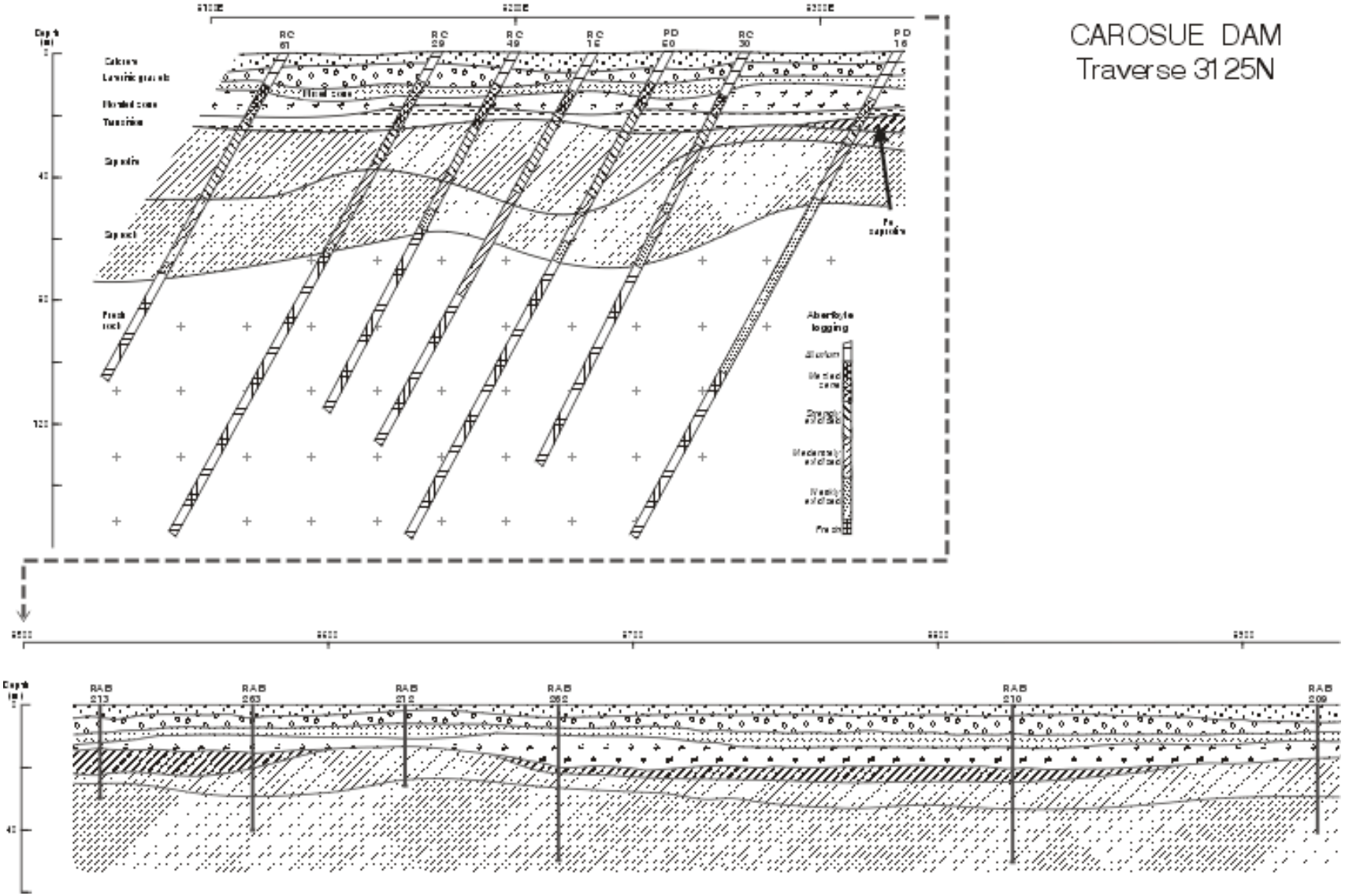

Figure 10: Summarized CRC LEME and Aberfoyle logging information for Carosue Dam Section 3125N

4. GOLD GEOCHEMISTRY / 3D MODELLING

4.1 Results for the 3125N Traverse

Examination of the Au geochemistry across traverse 3125N (Figure 11) indicates several zones of Au remobilization in the regolith. Mineralization extends upwards through the fresh rock and the saprock (weakly and moderately oxidised zones. Depletion occurs at the saprock-saprolite (moderate-strongly oxidised) boundary. Note that the depletion front appears to follow this boundary, rather than occur at a certain elevation. Just below this depletion front, Au is enriched, suggesting that some of the leached Au has been reprecipitated just below the depletion front. Closer to the surface, Au remains low, with the exception of the surface calcrete, which is Au-enriched.

Thus results from this traverse suggest strong lithological control over Au remobilization. These conclusions are confirmed in 3D calculations for the entire area (Sections 4.2 and 4.4).

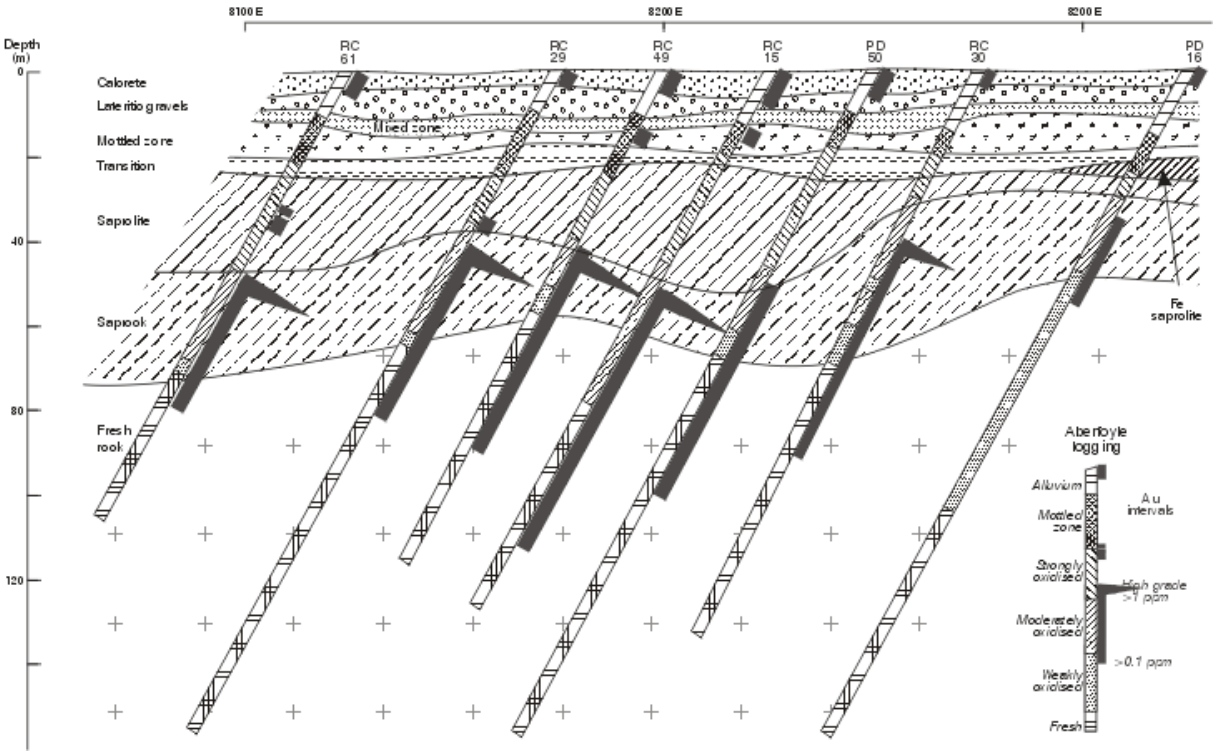

Figure 11: Gold geochemistry for Carosue Dam Section 3125N

4.2 Raw data Au concentration calculations

Initial investigations on the raw geochemical data clearly are biased by a greater sampling density in the central mineralized zone, but will not have been smoothed by gridding (see below). Gold concentrations were combined into each metre RL and the mean (Figure 12) and geometric mean (Figure 13) Au grade plotted vs. mRL. The zone between 330 and 355 mRL is clearly much poorer in Au (Figure 12), indicating depletion, and transported cover at the top. There is a clear surface enrichment at 355 – 362 mRL (Figure 12; note that the apparent peak in Au concentration 4 m below the highest elevations is due to the data being graphed vs. RL rather than depth from a surface (which has a variation of 9 m over the study area; Figure 4), and that much of the surface data is from 4 m composites), with values up to 400 ppb Au recorded. Comparing Figure 12 and Figure 13 indicates that the geometric mean overestimates the surface anomaly, relative to the underlying mineralization. This is due to the surface material having a more normal distribution than at depth; thus, for the surface the geometric mean is

more than half the arithmetic mean, whereas for the deeper mineralized zone the geometric mean is less than a fifth the arithmetic mean. This indicates significant redistribution of the surface Au.

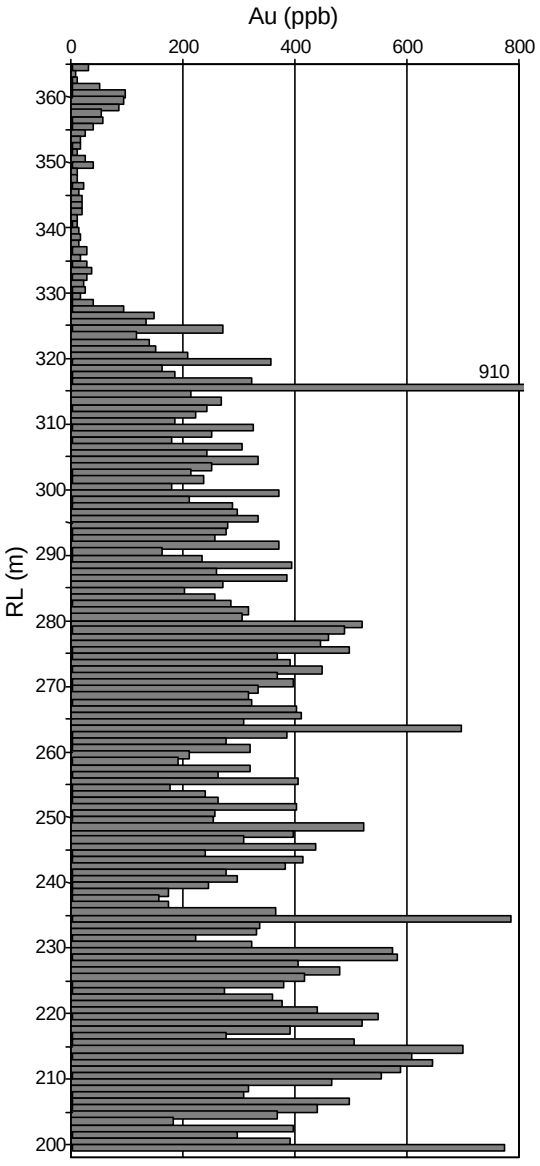

Figure 12: Mean Au grades (raw data) vs. mRL depth.

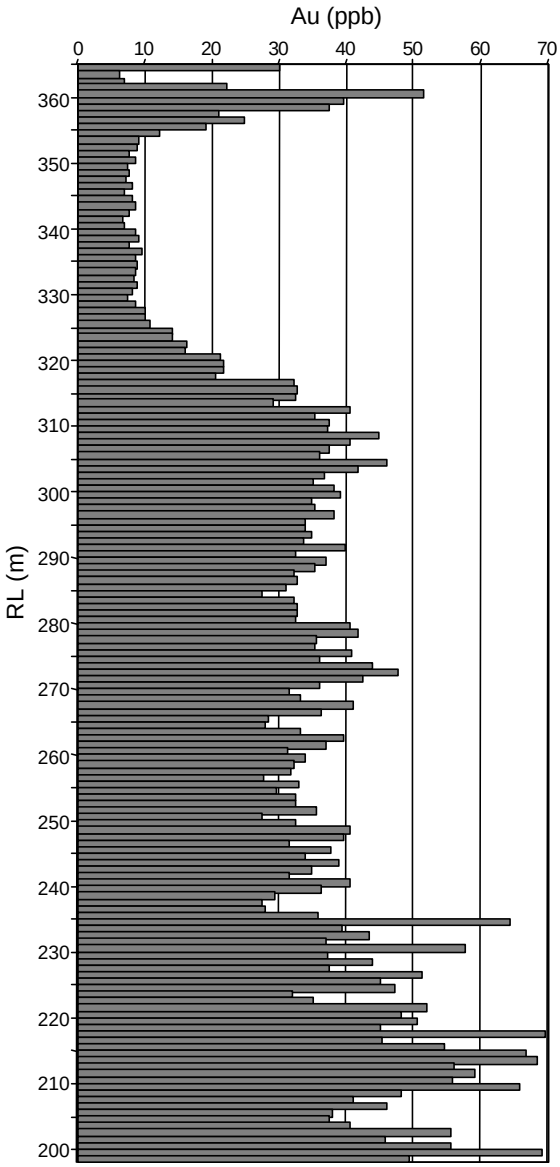

Figure 13: Geometric Mean Au grade (raw data) vs. mRL depth

4.3 MVS calculations of Au concentrations

The average thickness of the *in situ* horizons at Carosue Dam – ferruginous zone (14.2 m), strongly- (19.1 m), moderately- (15.4 m) and weakly-oxidised saprolite (15.5 m) - are similar (Figure 14). The transported sediments consist of 3 m calcrete overlying 5.7 m carbonate-poor alluvium. For the *in situ* materials, Au concentrations increase going from unweathered rock (232 ppb), to the moderately-oxidised horizon (325 ppb), with a major decrease in the strongly oxidised saprolite (47 ppb) and ferruginous zone (28 ppb) (Figure 15). The transported sediments are also relatively Au-poor, though there is a significant increase from the alluvium (27 ppb) to the overlying calcrete (60 ppb).

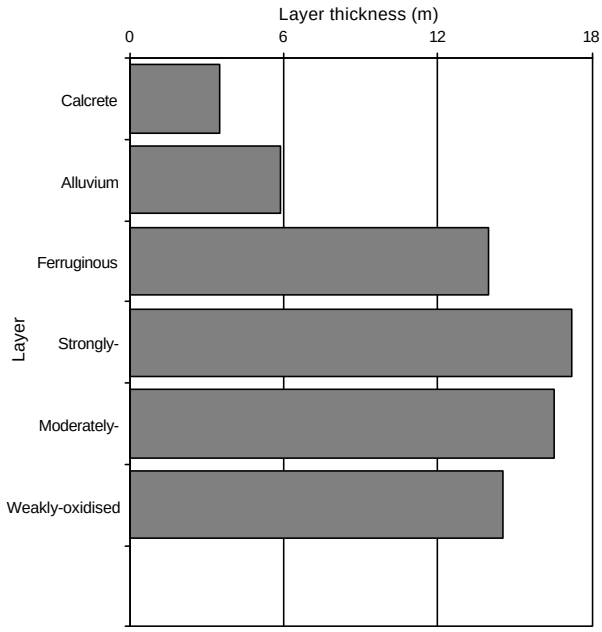

Figure 14: Thicknesses of each regolith layer, Carosue Dam.

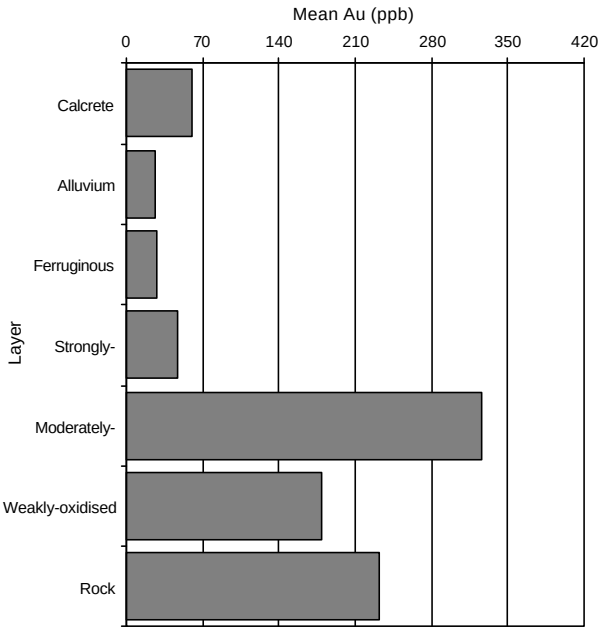

Figure 15: Mean Au for each regolith layer, Carosue Dam.

On the basis of the observation that the Au depletion front occurs at the strong-moderately oxidised transition (Section 4.1), the strongly oxidised zone was split into a 'base' (lower 6 m) and 'top' (the rest) and the moderately oxidised zone was similarly split into a 'top' (upper 6 m) and 'base' (Figure 16). The base of the moderately oxidised zone has the highest Au concentration (348 ppb), with decreasing concentrations upwards to a very low Au content (27 ppb) in the top of the strongly oxidised zone (Figure 17). This suggests that the upper strongly oxidised and ferruginous zones (with a combined thickness greater than 25 m) are approximately 90% depleted relative to the moderately and weakly oxidised zones.

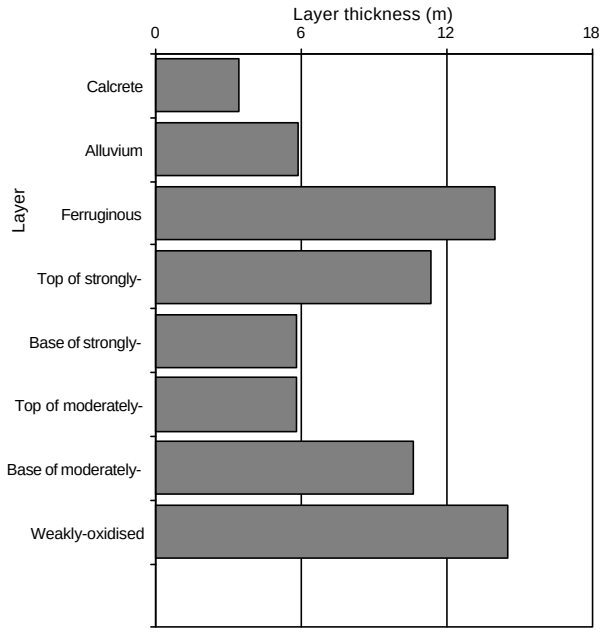

Figure 16: Thicknesses of regolith layers optimised for Au concentration discrimination, Carosue Dam.

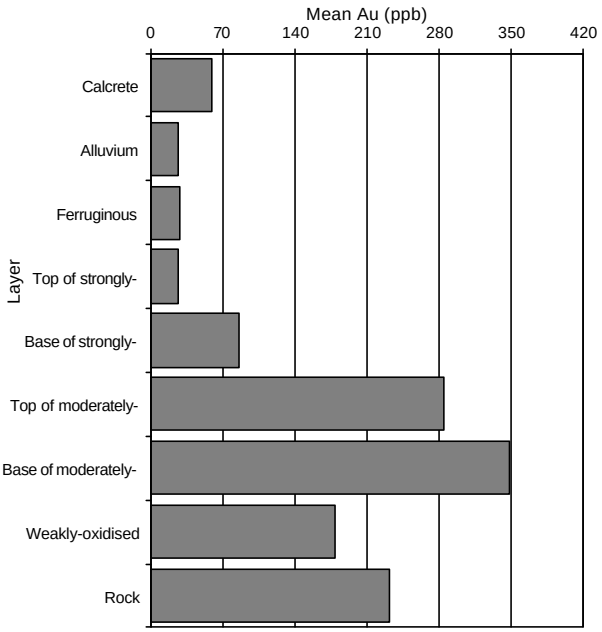

Figure 17: Mean Au of regolith layers optimised for Au concentration discrimination, Carosue Dam.

Further calculations of mean Au for Carosue Dam are based on 3 m thick slices taken above and below the various regolith transition and from the surface, with additional analyses based on 0.5 m thick slices also performed across the moderate-strongly oxidised transition. The reliability of the results of each slice has been calculated using the method described in Section 2.2. Only those slices considered 60% reliable or greater were used.

Calculations of mean Au content as a function of distance from the weathering front were done for the entire *in situ* rock and regolith, and for the thinner weakly oxidised horizon only, with both sets of data shown in Figure 18. Only 4 data points, spanning 0 – 12 m upwards from the weathering front, were available for the weakly oxidised horizon only, and did not indicate any clear effect. Data for the entire *in situ* regolith show a major depletion occurring between 25 – 40 m above the weathering front. Similarly, mean Au content relative to the weak-moderately oxidised transition (Figure 19) was calculated for all *in situ* material and for the moderately and weakly oxidised materials only. The later data shows a clear increase in Au content across this transition, which is more muted when Au content is calculated for all *in situ* material. At greater than 10 m above this transition, Au content decreases considerably, from greater than 350 ppb approximately 10 m above the transition, to <40 ppb Au more than 30 m above the weak-moderately oxidised transition.

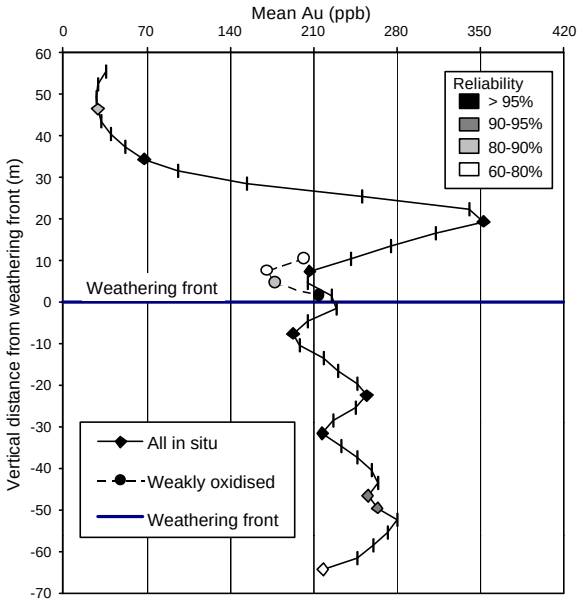

Figure 18: Mean Au vs. distance from the weathering front, Carosue Dam.

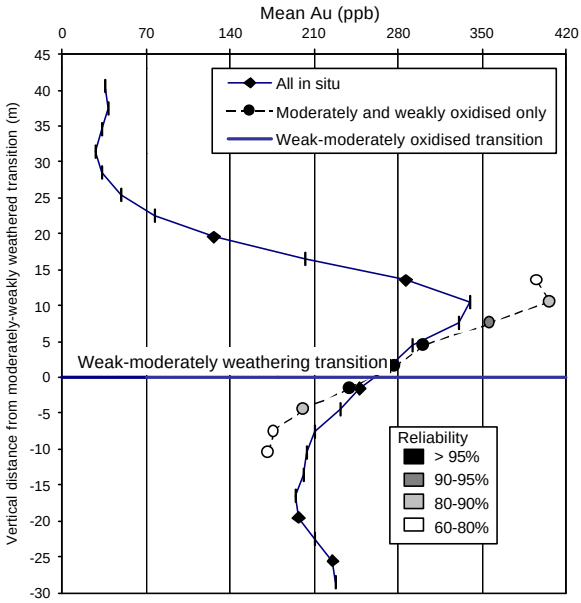

Figure 19: Mean Au vs. distance from the weakly to moderately oxidised transition, Carosue Dam.

The increase in Au concentration 10 m above the weak-moderately oxidised transition (Figure 19) is observed as an increase approximately 11 m below the moderate-strongly oxidised transition (Figure 20). This increase is significantly greater (400 ppb Au) when the moderately oxidised zone is considered alone, than for the entire *in situ* material (up to 345 ppb Au). Above this enrichment zone, there is a major Au depletion occurring 10 m either side of moderate-strongly oxidised transition (Figure 20), with Au concentration reducing to 25 ppb at and above the pedoplasmation front (Figure 21). Gold concentrations actually increase up through the unconformity (Figure 22; though note change in Au concentration scale), reaching a maximum of 60 ppb in the calcrete (Figure 23 and Figure 24).

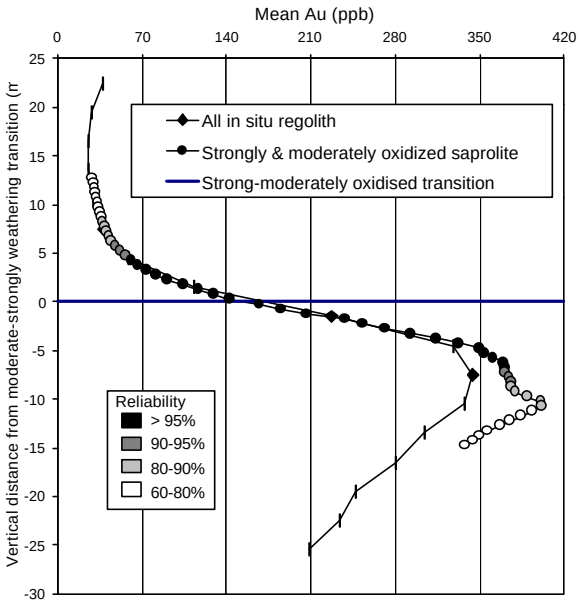

Figure 20: Mean Au vs. distance from the moderately to strongly oxidised transition, Carosue Dam.

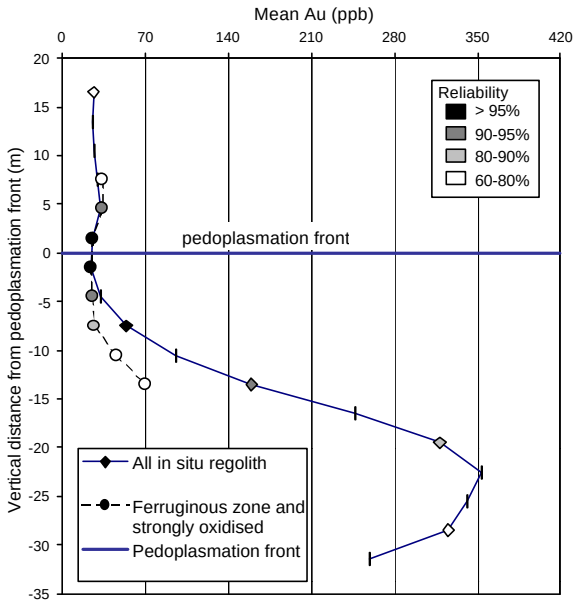

Figure 21: Mean Au vs. distance from the pedoplasmation front (base of ferruginous zone), Carosue Dam.

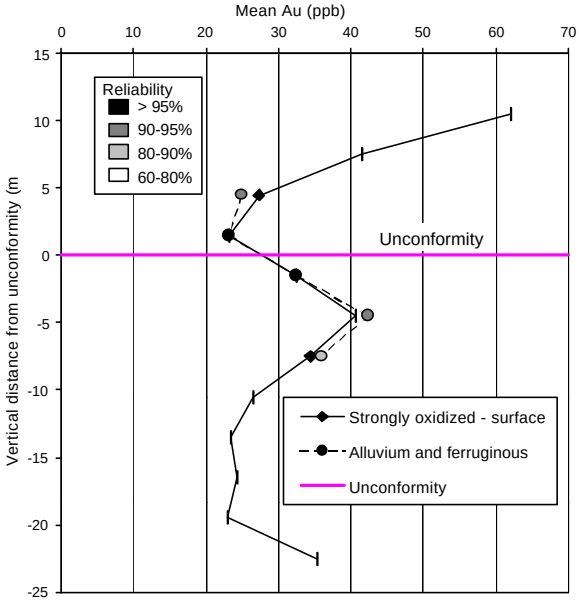

Figure 22: Mean Au vs. distance from the unconformity, Carosue Dam.

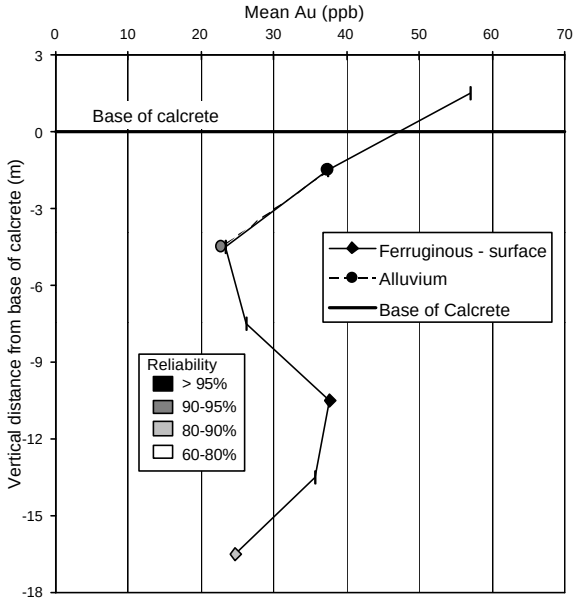

Figure 23: Mean Au vs. distance from the base of calcrete, Carosue Dam.

Calculations of Au concentrations in the residual regolith as a function of elevation (Figure 25), show variations of 190 - 280 ppb Au between 220 and 280 m elevation, which are the depths dominated by unweathered rock. Above this elevation, Au content continues to fluctuate, though more extreme variation is observed if the values for the weakly and moderately zones (triangles in Figure 25) are used. Marked Au depletion is observed above 315 mRL, with both the strongly oxidised saprolite (diamonds) and the ferruginous zone (circles in Figure 25) having low Au. The relative depletion is greater than 85%. Virtually identical results were observed for 0.5 m slices. However, though the features observed

by studying successive slices away from the regolith transitions (Figure 18 - Figure 21) are also seen by taking elevation cuts (Figure 25), the magnitude of the variations are greater if Au content is measured vs distance from regolith transitions (particularly see Figure 20) or if differing units analysed separately (note the extreme contrast between strongly oxidised and moderately/weakly oxidised units in Figure 25) than if determined vs. RL. This suggests that the Au depletion is controlled more by the regolith surfaces than by processes that are purely a function of elevation. This is consistent with the observations made for traverse 3125N (Section 4.1, Figure 11), that the depletion and enrichment are controlled by the saprock-saprolite boundary, rather than a certain elevation.

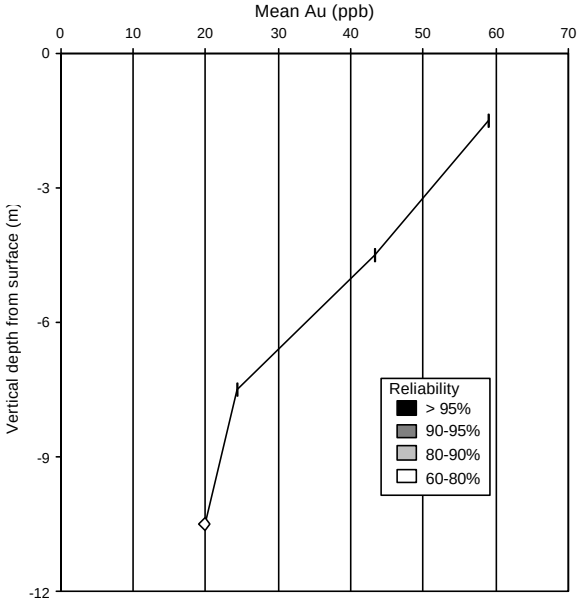

Figure 24: Mean Au vs. depth from surface for transported overburden, Carosue Dam.

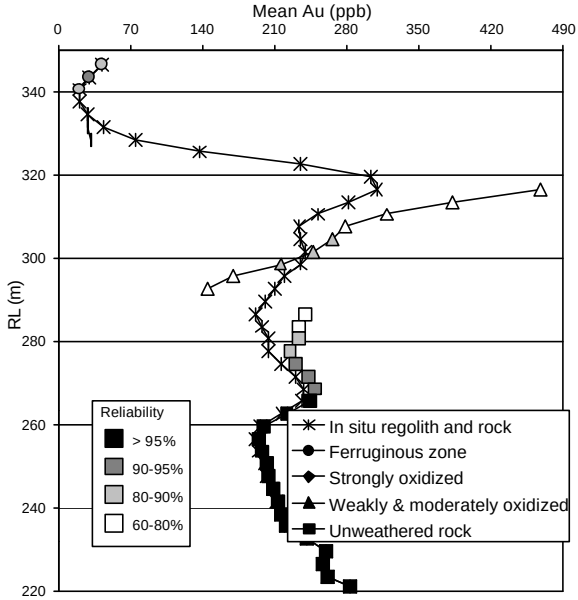

Figure 25: Mean Au vs. elevation for Carosue Dam.

Comparisons of Figure 12 and Figure 25 show general similarity, though the results for Figure 25 are much smoother, as expected for gridded data with 3 m, rather than 1 m, slices.

4.4 Visualisations of Au concentration

The lateral distribution of Au below the depleted zone (*e.g.*, at 300 mRL in Figure 26) shows the major Au grades to occur in the north of the study area (3000 - 3500 mN) though with some high grade pockets in the south. The location of the major Au mineralization can be observed faintly in the overlying depleted zone (*e.g.*, at 340 mRL in Figure 27). The highest surface Au grades occur between 2600 and 3100 mN (Figure 28), with the highest grades corresponding with the area of greatest Au in the depleted zone (Figure 27). If the surface Au is derived from this resistant Au shoot, this implies that the Au to the north and south has been translocated several hundred metres to the south. The translocation to the south is upslope (Figure 4), and is therefore less likely to be due to physical movement. This will be discussed further in Section 7.

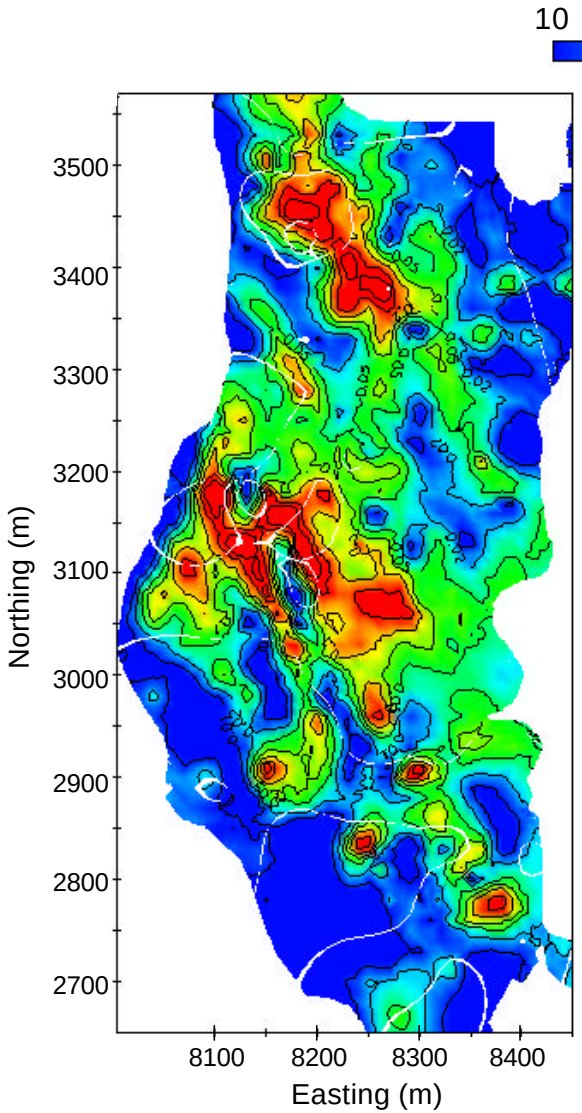

Figure 26: Contoured Au data at 300 mRL (below depleted zone), Carosue Dam.

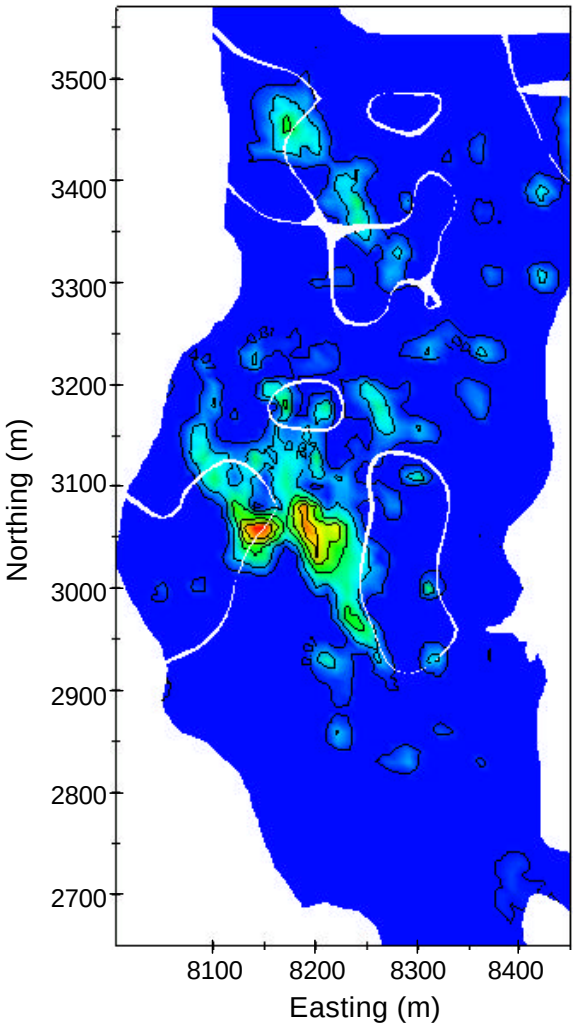

Figure 27: Contoured Au data at 340 mRL (depleted zone), Carosue Dam.

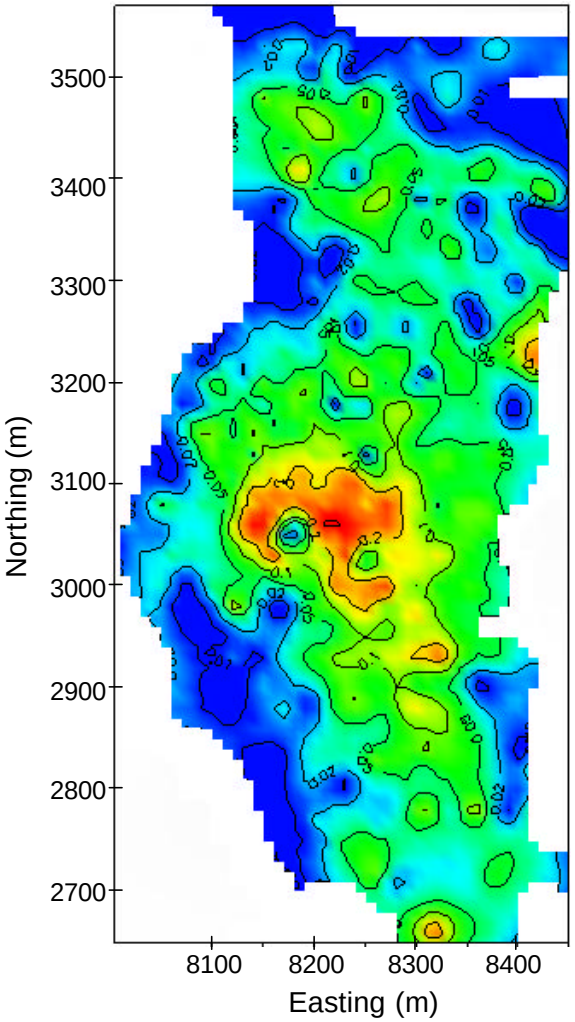

Figure 28: Contoured Au data for the regolith surface, Carosue Dam.

Gold data was kriged as described in Section 2.1. Various plots are included as bitmap files in the accompanying CD, in separate directories, as described briefly below, and listed in Appendix 1:

(i) The SliceN directory includes vertical slices at constant northing, with plots named according to the particular northing.
(ii) The SliceE directory includes vertical slices at constant easting, with plots named according to the particular easting. Thus the plot shown in Figure 30 is named 8200mE.BMP.
(iii) The Cut-offs directory includes the various layers coloured as in Figure 5, either merged together to show the true stratigraphy (LAYERS.BMP), exploded as in Figure 5 so as to show the characteristics of the various layers (EXP_AU.BMP), or with a particular Au grade cut-off (thus the plot shown in Figure 29 is named 50PPBAU.BMP).
(iv) The Plans directory includes plans of regolith distribution or calculated Au grade at a particular RL (*e.g.*, the plot of the calculated Au concentrations at 300 mRL is named 300MRL-AU.BMP) at a particular surface (*e.g.*, the plot of the calculated Au grade at the unconformity is named UNCONF-AU.BMP) or at a set vertical distance from a weathering surface (*e.g.*, the plot of the calculated Au grade 2 m below base of weathering the is named BOW-2-AU.BMP).
(v) The Interactive directory includes interactive 3D models written with Virtual Reality Modelling Language (VRML) which can be manipulated by the user (rotate, pan, zoom) and simply require an internet browser (Netscape, Explorer, no outside line necessary) with a plug-in that is provided on the report CD. See Appendix 1 for details.

The various characteristics briefly described in Section 4, namely the ore zone in the north of the study area, the depleted zone and the carbonate Au-enrichment are observed in the cut-off diagrams (Figure 29), vertical slices (Figure 30) and by comparing Au grade at various depths (CD, PLANS directory). The major depletion occurs down to 330 mRL and closely matches the base of strongly oxidised zone: *i.e.*, the strongly oxidised zone, ferruginous zone (as defined in Section 2.1) and transported cover (though not the carbonate zone) are all Au-poor.

Analysis of Figure 29 offers some possible explanations for the origin of the carbonate Au anomaly. As stated previously (Section 4), the surface Au anomaly matches underlying mineralization at approximately 3000 mN, with a surface anomaly overlying poorly mineralized rocks southwards and poor surface expression of mineralization northwards. This can be observed as the minor expression of mineralization within the ferruginous zone (the red column) at approximately 3100 mN, which visually appears to supply Au to the surface. North of 3000 mN, there is a significant decrease in thickness of the ferruginous zone (Figure 7), possibly representing truncation of the (once) Au-rich gravel layer, and thickening of the transported cover (Figure 6) from 8 - 10 m to > 12 m. Thus the area at 3000 - 3100 mN represents the only part of the study area with conditions conducive to a Au signal at surface: *i.e.*, mineralization through the elsewhere depleted zone, moderately intact residuum and less than 10 m transported cover. Results compare with those from Safari (Bristow *et al.*, 1996b), where transported cover was 5 - 10 m thick, with good Au responses in the carbonate horizon above the unconformity.

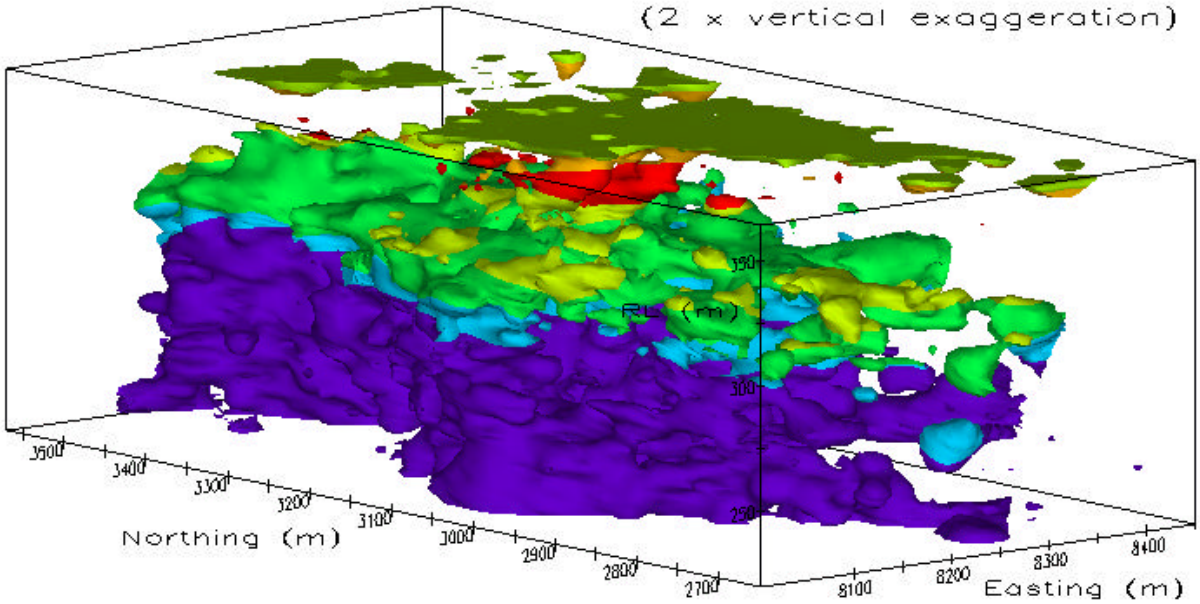

Figure 29: Gold distribution using a 0.05 ppm cut-off, Carosue Dam. Thus, where Au is greater than 0.05 ppm, the area will be coloured according to the regolith horizon: purple - rock, blue - weakly oxidised saprolite, green - moderately oxidised saprolite, yellow - strongly oxidised saprolite, red - ferruginous zone (Section 2.1), orange - transported cover, yellow/green - carbonate zone.

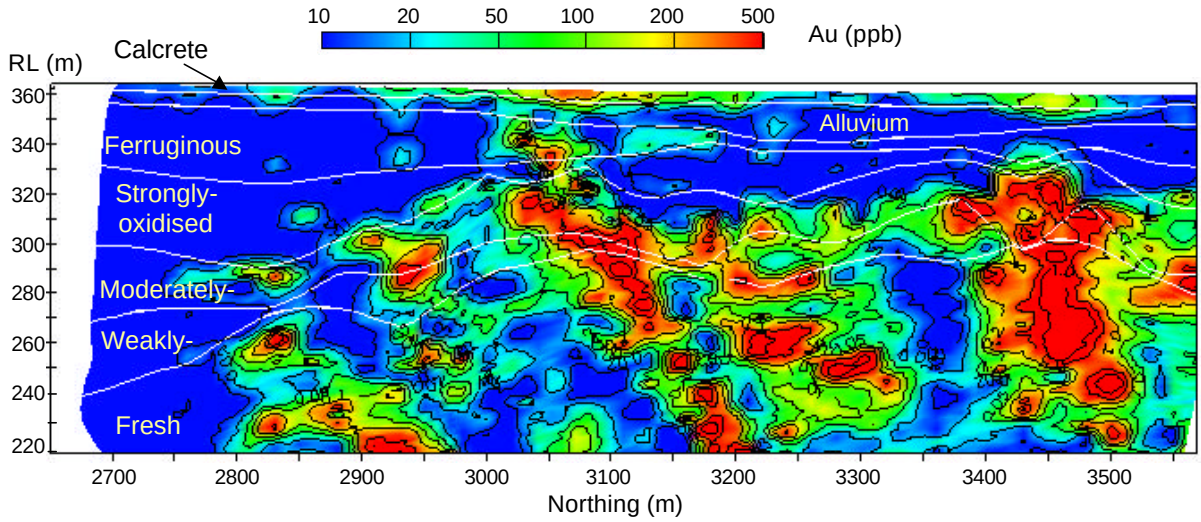

Figure 30: Calculated Au grade for 8200 mE traverse, Carosue Dam (2x vertical exaggeration).

The hypothesised processes leading to the observed supergene Au distribution at Carosue Dam are shown diagrammatically in Figure 31. During laterization in the Tertiary, Au could have been dispersed into the surface laterite away from the ore body (Figure 31A). To the north, this laterite cover would have been lost during later erosion, with thicker deposition of alluvium than in the southern part of the study area (Figure 31B). With the more extensive laterite and the lesser transported cover, a surface Au signature could be readily formed to the south. Since the Tertiary, surface groundwaters have become corrosive for Au (Section 6.6), and Au has been leached down to the strongly to moderately oxidised transition (*i.e.*, the major Au depletion approximately corresponds to the strongly oxidised saprolite and the ferruginous zone).

Examination of Au distribution below, at and above the base of weathering show little indication of Au dispersion during initial weathering (see accompanying CD), though a small amount of mobility would be difficult to see due to the primarily dispersed nature of the mineralization.

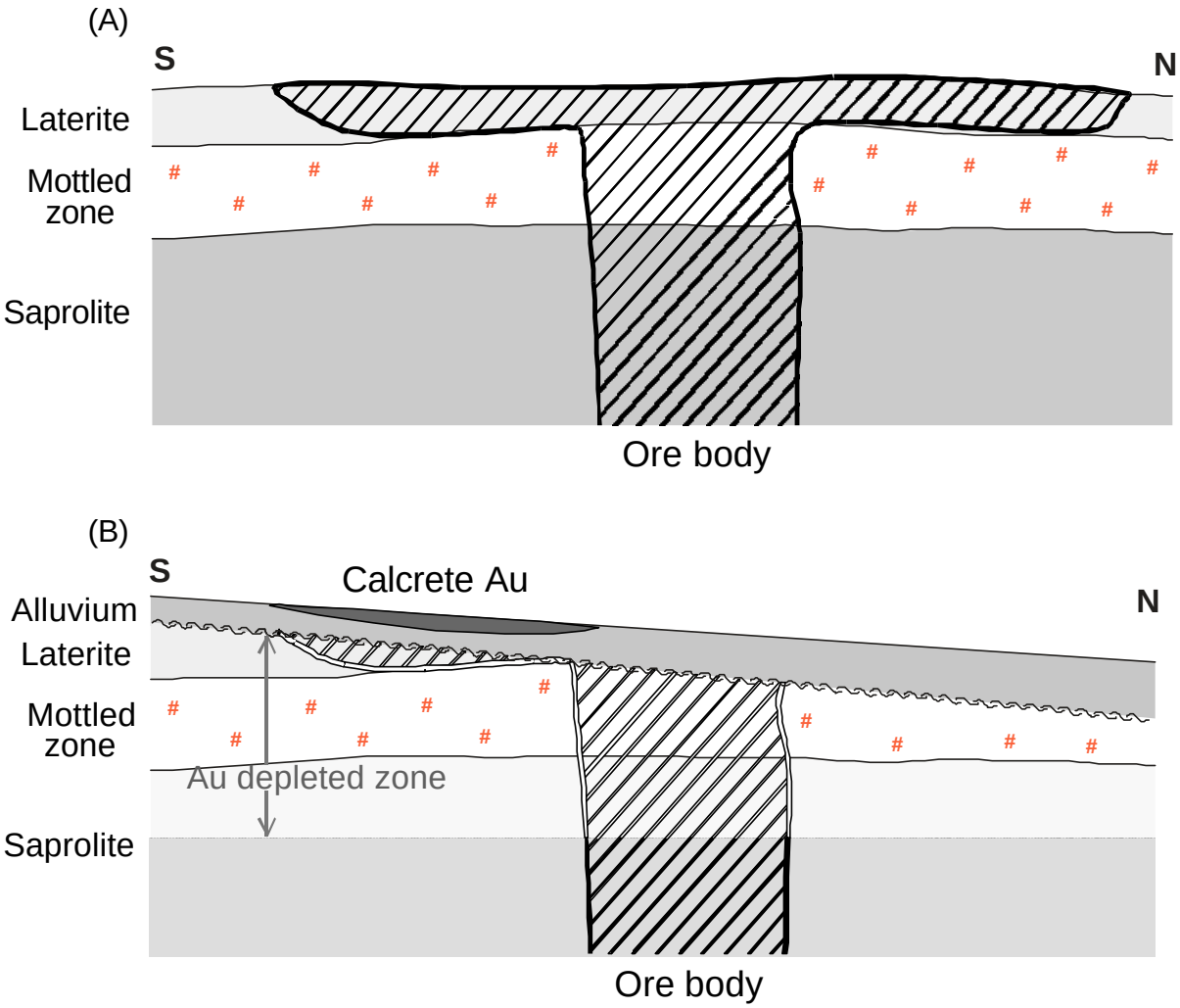

Figure 31: Possible origin of surface Au anomaly at Carosue Dam: (A) Tertiary weathering with dispersion of Au into laterite; (B) Stripping of laterite to the north, deposition of alluvium with soil Au anomaly in the south, and leaching of buried Au above strongly to moderately oxidised transition.

5. CHARACTERISTICS OF PARTICULATE GOLD AT CAROSUE DAM

5.1 Introduction

Gold grains were extracted from 10 bulk samples taken from drill spoils along the 3125N line. The samples were taken from the subsurface anomaly, the saprolite dispersion halo and the primary mineralization (Table 2, Figure 32). The samples were separated using techniques describing in Section 2.3, with results discussed below and photos of the Au grains enclosed in the Appendices.

Table 2: Gold concentration of the bulk samples, with sample numbers as used *in Figure 32*

Regolith zone	Sample	Drill hole	Depth (m)	Gold grade (ppm)
Calcareous colluvium	A	49	1-2	0.28
	B	49	4-5	0.52
	C	50	1-2	0.48
Lower saprolite	D	61	40-41	0.15
	E	49	48-49	32.3
	F	15	59-60	10.3
	G	30	45-46	1.5
	H	16	48-49	2.5
Primary mineralization	J	49	110-111	5.1
	K	50	105-106	7.2

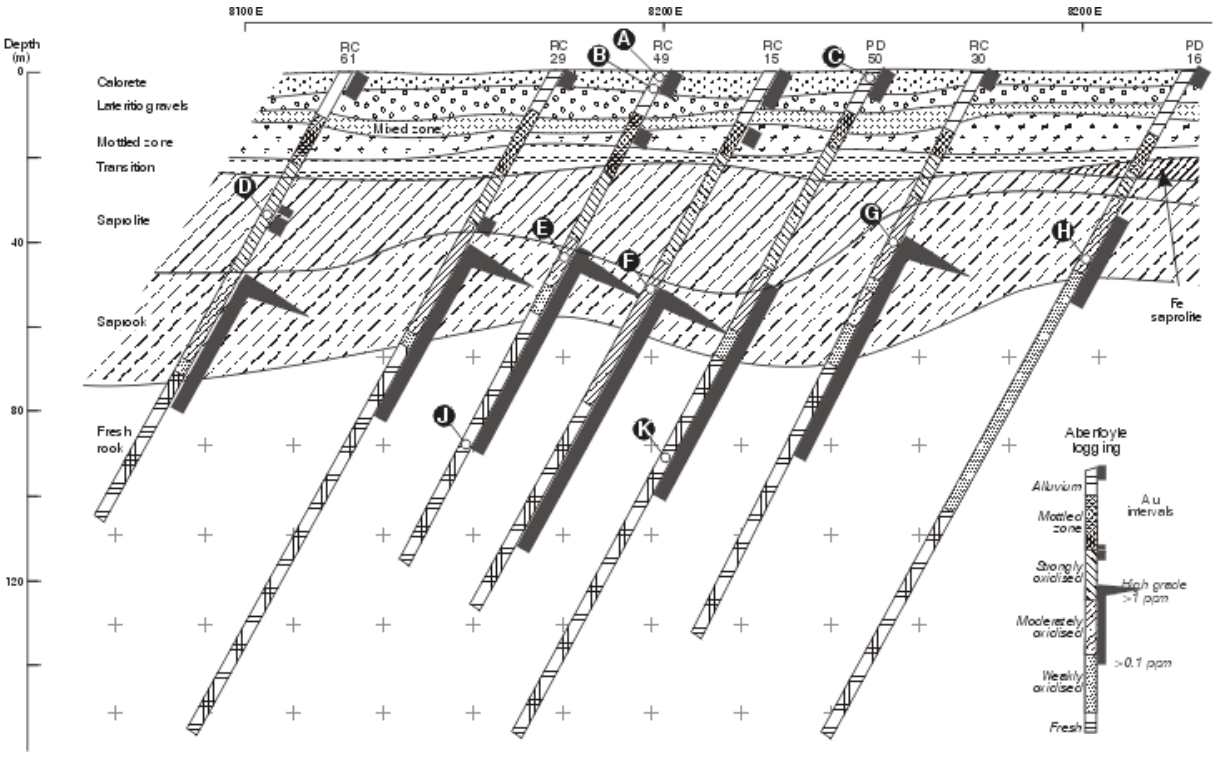

Figure 32: Position of Au grain sampling, from Carosue Dam Section 3125N

5.2 Characteristics of gold grains

5.3 Primary mineralization

Gold grains are small in the primary mineralization (Samples J and K), with 80 - 85% less than 100 µm diameter, and only 2-5% exceeding 200 µm. Most grains are irregular and xenomorphic, with minor

occurrence of equant and elongated grains and flakes (Photo 1). The surfaces of the primary grains are rough, with numerous cavities, fractures, scratches and imprints from adjacent minerals. Some of the scratches are probably the result of mechanical damage to the grains during drilling and sample preparation.

The principal minerals associated with Au in primary mineralization are pyrite and aluminosilicates, usually feldspar (Photos 2-3), with lesser quartz and calcite. All primary Au grains have up to 14% Ag content. Quantitative microprobe analysis of two Au grains shows 6.9 and 13.7% of Ag, 210 and 140 ppm of Cu and 160 and 140 ppm of Si respectively (Table 3).

Below the sub-horizontal front of weathering, some small high fineness Au crystals, (4-10% of total grains) are presumably supergene (Photo 1). These Au crystals appear to form as a result of deeper weathering along fractures, with chemogenic Au transport and deposition at least 30 m below the weathering front. Sporadic occurrences of Fe oxides as intergrowths with Au crystals and films at the pyrite grain surface corroborate this hypothesis.

Table 3: Comparative characteristics of the primary and supergene Au, Carosue Dam

Gold type	Grain length <100 µm, %	Shape	Composition (EMPA)		
			Ag (%)	Cu (ppm)	Si (ppm)
Primary (2 samples)	80	Irregular, xenomorphic grains	6.9 - 13.7	140 - 220	140 - 160
Supergene (5 samples)	100	Prismatic, tabular crystals	Bdl (150 ppm)	Up to 30 ppm	140 - 290

Fe and Pd concentrations below detection limit (Bdl)

5.4 Gold dispersion halo within saprolite

Gold grains are smaller in this zone than in the primary mineralization, with 90 to 100% (mean 96%) of the grains less than 100 µm in diameter. In contrast to the primary mineralization, Au crystals are predominant (50-70%, mean 61%) within the dispersion halo, except for the residual mineralized zone, where the proportion of crystals is 22%.

The majority of the Au crystals are subhedral, with euhedral crystals less common. Prismatic and tabular crystals are predominant, with rare elongated crystals and combinations of cubic and octahedral forms (Photos 4-8). Commonly, complex aggregates occur, composed of subhedral crystals or unclear crystalline grains. Pristine crystals are rare, and crystals with rough surfaces, pits, cavities and imprints from adjacent minerals are common. Some crystals and grains are corroded (Photo 5). All the crystals in the zone are of high fineness and contain no Ag (detection limit 150 ppm) and only 140-290 ppm of Si (Table 3). Only one in nine analysed Au crystals has Cu and Fe at the detection limit (30 ppm), with the other crystals below detection.

Supergene gold is mainly associated with Fe oxides, forming complex intergrowths or being covered by films of Fe oxides. Inclusions of quartz and silicates are less common (Photo 6). Similar to adjacent Twin Peaks site, one of the supergene Au crystals studied has complex intergrowths with phase of Ca - P composition, presumably apatite (Photo 8).

5.5 Subsurface anomaly

Gold grains from calcareous colluvium are small in size, with 99-100% particles less than 100 µm. Gold occurs mainly as irregular and equant grains (35-55%) and crystals (27-47%). The crystals are commonly uncorroded, in contrast to irregular grains which show moderate to strong corrosion (Photos 9-12). Corroded Au grains contain some Ag and presumably are relic primary Au. Among residual Au grains some relic primary minerals (pyrite and cinnabar) were identified. No specific Au morphologies that could be related to Au redeposition in the calcrete environment were detected.

5.6 Discussion

Gold in the regolith at the Carosue Dam is quite similar to that in many other studied sites in the Yilgarn Craton (e.g. Freyssinet and Butt, 1988; Gedeon and Butt, 1990; Lawrance and Griffin, 1994; Porto et al., 1999). Primary Au grains are irregular and xenomorphic and tend to be 950 fine or less, alloyed with Ag and trace amounts of other elements (e.g. Cu, Hg, Te, S).

Unlike the primary Au, free supergene Au mainly occurs as small crystals of high fineness with very low or no detectable Ag and other admixtures. Some supergene Au particles contain trace Fe, S and As. The supergene Au has many crystal forms, with the most common varieties as follows:

combinations of cubes, octahedra and dodecahedra, elongated in one of the axes;
very thin platy pseudo-hexagonal and triangular crystals.

In a broad sense, the crystal shape of a mineral is a function of the environment. One of the hypotheses on supergene Au, based on the experimental study of Gatellier and Disnar (1988) was that supergene Au crystal shape is dependent on groundwater salinity (Butt, 1991). For example, thin platy crystals were found in the highly saline environment of the Hannan South (Lawrance and Griffin, 1994) and Panglo deposits (Scott and Davis, 1990). Gold grain studies performed within previous CSIRO projects as well as the P504 do not at present support this idea. Despite different hydrogeochemical characteristics of Mt Joel, Panglo and Old Plough Dam area (Twin Peaks, Monty Dam and Carosue Dam), the supergene Au morphologies are very similar: Au mainly occurs as tabular and prismatic crystals at these sites (Scott and Davis, 1990; Sergeev and Gray, 1999). One possible explanation is that Au transport in the past was by groundwaters different in salinity from the present studied ones.

Detailed investigations at Twin Peaks (Sergeev and Gray, 1999) and the study performed at Carosue Dam discussed here show that substantial proportions of Au within subsurface dispersion haloes are represented by relics of the primary Au, indicating at least in part residual Au concentration and mechanical transport near the surface. This observation is critical to the understanding of surface Au mobility in these environments.

6. HYDROGEOCHEMISTRY

6.1 Introduction

A primary justification given for the use of hydrogeochemistry in mineral exploration is that groundwater anomalies may be broader and more regular than mineralization and secondary dispersion haloes in the regolith, thus enhancing the geochemical signature. In addition, areas of high chemical reactivity (*e.g.*, faults and shear zones) may have distinct hydrogeochemical signatures even where the "solids" are unremarkable in terms of elemental abundances, and where petrographic study is difficult. Hydrogeochemical studies also provide information on how various materials are weathering. This enhances understanding of active dispersion processes and assists in the development of weathering and geochemical models, which are essential for effective exploration in regolith-dominated terrain.

Therefore, the aims of this hydrogeochemical study were:

(i) to yield data on geochemical dispersion processes, and to assist in interpretation of geochemical data;
(ii) to provide information on whether groundwater can be used successfully as an exploration medium in this area in particular and, in conjunction with other studies, in the central Yilgarn in general;
(iii) to check for differences in groundwaters contacting felsic rocks in comparison with other Archaean rock types;
(iv) to contribute to a groundwater database on the characteristics of groundwaters at various sites, and to enhance our understanding of groundwater processes in mineralized zones.

The scope of this investigation includes the effect of underlying lithology on the observed water chemistry, thermodynamic modelling, mapping of the data and comparison with results from other Western Australian sites.

6.2 Compilation of results and comparison with other sites

The concentrations of various ions at Carosue Dam and at other sites are plotted versus TDS, pH or Eh in Appendix 2, Figures A2.1 - A2.46. The sea water data (Weast, 1983) are used to derive the line of possible values (denoted as the sea water line) if sea water (TDS 3.5%) were diluted with freshwater or concentrated by evaporation; the line is shown on each figure except where the concentration in sea water is too low, relative to the concentration of the element in groundwaters to be observable. The results from Carosue Dam can be compared with those from other sites in southern WA, which are grouped as follows:

(i) *Northern groundwaters* (N Yilgarn and margins) -
Lawlers (Gray, 1994) and Baxter (Gray, 1995).
Groundwaters in these areas are fresh and neutral, trending more saline in the valley floors.
(ii) *Central groundwaters* (close to and north of the Menzies line) -
Granny Smith (Gray 1993a), Golden Delicious (Bristow *et al*., 1996a), Mt. Gibson (Gray, 1991) and Boags (Gray, 1992a)
Groundwaters are neutral and brackish (commonly < 1% TDS) to saline (about 3% TDS), trending to hypersaline (10 - 30% TDS) at the salt lakes, with common increases in salinity with depth.
(iii) *Kalgoorlie groundwaters* -
Golden Hope mine, (Gray, 1993b), Wollubar palaeochannel (Gray, 1993b), Panglo deposit (Gray, 1990), Baseline mine, Mulgarrie palaeochannel (Gray, 1992b), Steinway palaeochannel (Lintern and Gray, 1995a) and Argo palaeochannel (Lintern and Gray, 1995b).
These groundwaters are commonly acid (pH 3 - 5), except where buffered by extremely alkaline materials (*e.g.*, ultramafic rocks), and saline within the top part of the groundwater mass, trending to more neutral (pH 5 - 7) and hypersaline at depth and where within a few kilometres of salt lakes.

(iv) *Officer Basin* -
Mulga Rock palaeodrainage system (Douglas *et al*., 1993).
Groundwaters are saline to hypersaline and neutral to acid. The major ion chemistry is similar to that of the Kalgoorlie region, but the dissolved concentration of many other ions is low, due to sorption on lignites in the channel sediments.

Wollubar, Baseline and Panglo are acid groundwater systems, whereas the other sites have dominantly neutral groundwater. Comparisons with other sites may be useful in indicating the significance of any particular element anomaly, and whether the groundwater composition is affected by particular lithological interactions. Specific descriptions of the varying sites are found in the referenced reports, with generalized descriptions of the hydrogeochemistry of the Yilgarn Craton given in Gray (1996) and Butt *et al*. (1997).

Saturation index (SI) values for various minerals (Section 2.1) are plotted in Appendix 3, Figures A3.1 - A3.30. The equilibrium point is shown as a dashed line. The shaded area denotes the zone in which waters may be in equilibrium with that mineral. Note that where a mineral has a very broad zone, this indicates significant uncertainty in the thermodynamic data for this mineral and/or calculation problems - *i.e.*, samples within that zone are not necessarily at equilibrium, though samples above or below the zone are out of equilibrium. In addition, the distributions of elemental concentrations are plotted in Appendix 4, Figures A4.1 - A4.30.

6.3 Acidity and oxidation potential

An Eh-pH plot of waters from Carosue Dam and other sites is shown in Figure 33, along with the particular redox couples controlling groundwater Eh and pH, namely:

Fe - controlled by redox reactions between dissolved Fe^{2+} and Fe oxides
Mn - controlled by redox reactions between dissolved Mn^{2+} and Mn oxides
Al - controlled by reactions between dissolved Al^{3+} and kaolinite and other aluminosilicates.

These redox couples are described in detail in Gray (1996). Groundwaters are combined into the various groups, as described in Section 6.2. The Carosue Dam groundwaters are acid (pH 3.2 - 6.0), except for a single neutral (pH 7.1) sample in the SW of the study area (Figure A4.1), and range from moderately to highly oxidising, similar to the pH and Eh range of Kalgoorlie groundwaters, such as Panglo (Gray, 1990). Also included as the two parallel lines in Figure 33 are the Eh values for dissolution of Au: two of the groundwaters have Eh values high enough to allow dissolution of >2 µg/L Au, with another 3 groundwaters able to dissolve > 0.2 µg/L Au. As described below (Section 6.6), this is entirely consistent with the observed dissolved Au concentrations.

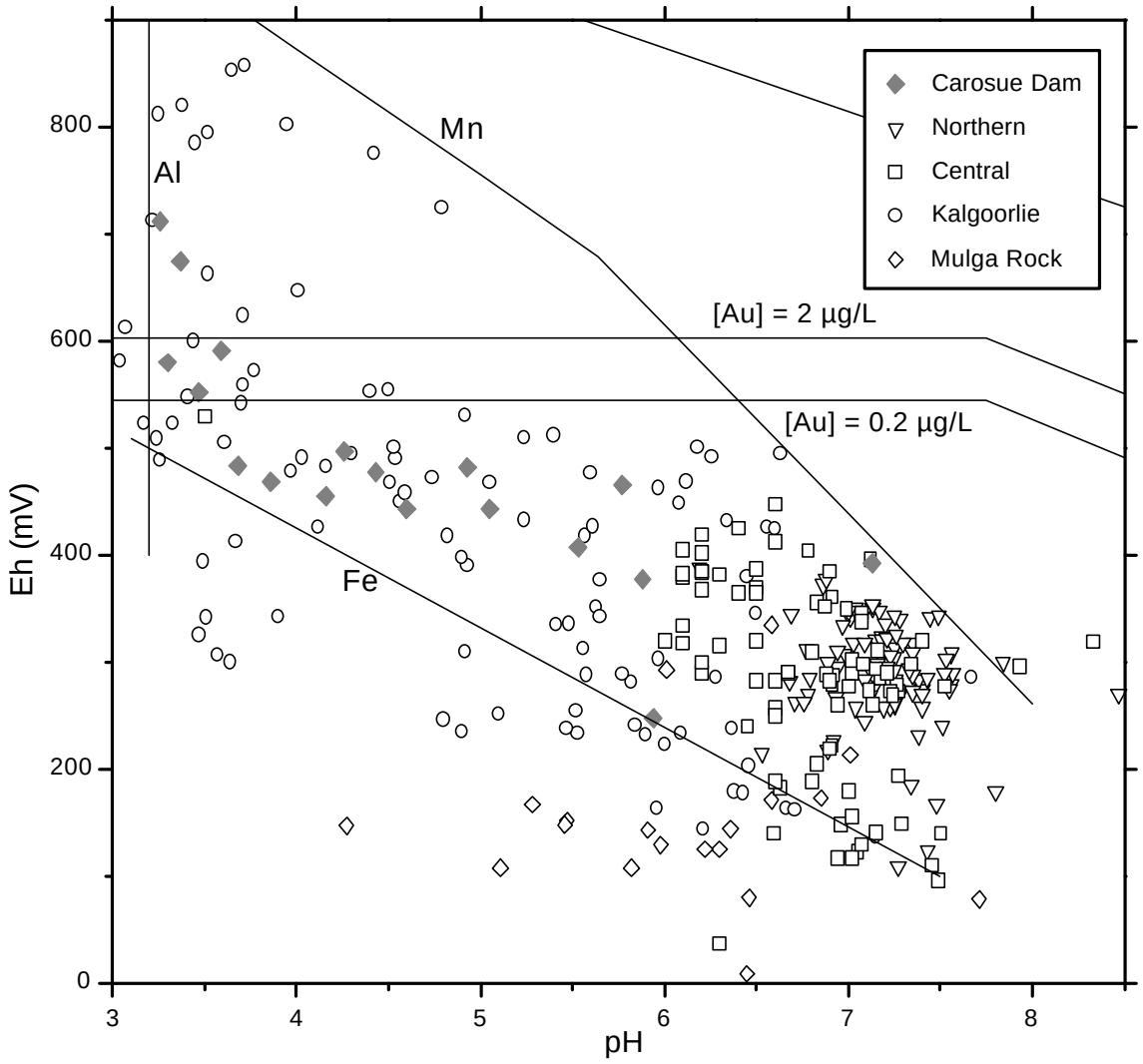

Figure 33: Eh vs. pH for groundwaters from Carosue Dam and other sites. Key: Fe - $Fe^{2+}/Fe(OH)_3$, Al - Al^{3+}/kaolinite, Mn - Mn^{2+}/Mn_xO_y.

6.4 Salinity effects and major element hydrogeochemistry

Data are plotted in Appendix 2, Figures A2.1 - A2.14. The Carosue Dam groundwaters range from saline (2.5% TDS, compared with sea water salinity of 3.5% TDS) to hypersaline (11.6%). The particular characteristics of the groundwaters at Carosue Dam are demonstrated by a plot of pH vs. TDS (Figure 34). Unlike the Central groundwaters, which have a wide range of salinities and remain neutral, the Carosue Dam groundwaters have pH variations similar to those of the Kalgoorlie groundwaters, though with significantly lower (by 2 - 3 times) salinities than the Kalgoorlie groundwaters. For most of the major groundwater elements (Na, Mg, Cl, SO_4), the element/TDS plots lie on a straight line defined by that for dilution or concentration of sea water (Figures A2.1, A2.3, A2.5 and A2.6): this implies that these groundwaters are in some manner (*e.g.*, by previous sea water incursion or from salt aerosol) sourced from sea water and then subsequently concentrated by evaporation. The Carosue Dam groundwaters are moderately depleted in Ca, relative to the concentrations expected if the groundwater had been diluted sea water (Figure A2.4), presumably due to gypsum and/or calcite precipitation. Additionally, these groundwaters show a significant K depletion, although not as great as that observed for Kalgoorlie (Figure A2.2). This is probably due to precipitation of alunite [$KAl_3(SO_4)_2(OH)_6$] in acid groundwater systems, as a by-product of the dissolution of kaolinite and other alumino-silicates (Gray, 1996). Alunite has been noted at several sites in the southern Yilgarn, *e.g.*, Panglo and Mt. Percy.

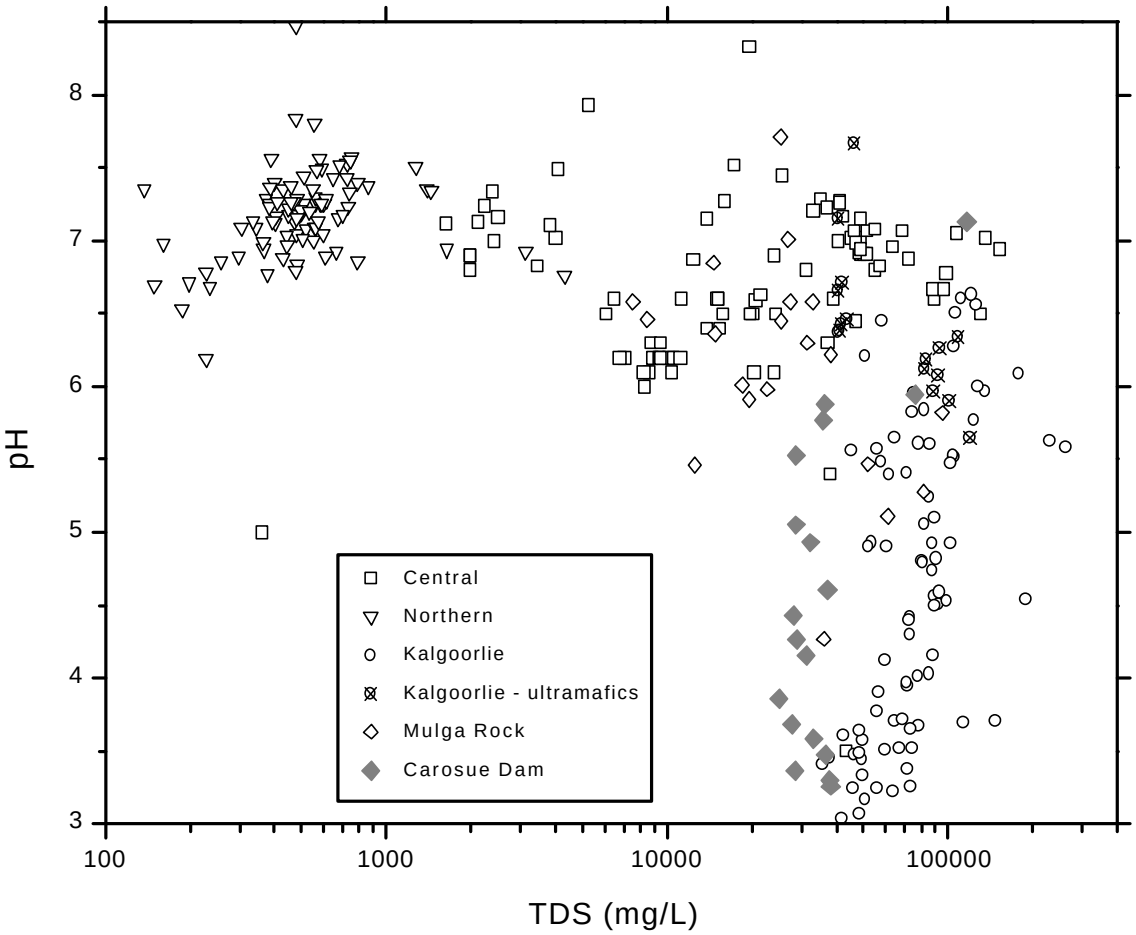

Figure 34: pH vs. TDS for groundwaters from Carosue Dam and other sites

The potential for dissolution or precipitation of minerals from groundwaters at Carosue Dam has been tested by speciation analysis (Section 2.1). The range, mean and standard deviation of the SI values of the water samples for a number of relevant solid phases are given in Table 4, with SI values plotted in Appendix 3. As discussed in detail in Section 2.1, in general, a SI of zero indicates the solution is saturated with respect to that mineral, a SI less than zero indicates under-saturation and a SI greater than zero indicates the solution is over-saturated with respect to the mineral phase.

Table 4: SI values for the Carosue Dam groundwaters, for a number of relevant solid phases

Mineral	Formula	No.	Min	Max	Mean	St Dev
Halite	$NaCl$	18	-2.8	-1.4	-2.5	0.3
Gypsum	$CaSO_4.2H_2O$	18	-1.2	-0.1	-0.9	0.3
Celestine	$SrSO_4$	18	-2.2	-0.4	-1.5	0.4
Barite	$BaSO_4$	18	-0.5	0.0	-0.3	0.1
Calcite	$CaCO_3$	8	-5.5	0.1	-2.8	1.7
Dolomite	$CaMg(CO_3)_2$	8	-9.5	1.4	-4.4	3.3
Magnesite	$MgCO_3$	8	-4.8	0.4	-2.4	1.6
Quartz	SiO_2	18	0.5	1.3	1.1	0.2
Amorphous silica	"	18	-0.7	0.0	-0.2	0.2
Gibbsite	$Al(OH)_3$	18	-2.1	2.8	0.0	1.6
Amorphous alumina	"	18	-4.3	0.5	-2.2	1.6
Alunite	$KAl_3(SO_4)_2(OH)_6$	18	0.1	9.0	4.6	2.4
Kaolinite	$Al_2Si_2O_5(OH)_4$	18	-0.9	8.2	3.1	3.0
Sepiolite	$Mg_2Si_3O_{7.5}(OH).3H_2O$	18	-14.6	0.0	-9.8	4.2
Siderite	$FeCO_3$	6	-6.1	-2.1	-4.6	1.4
Rhodochrosite	$MnCO_3$	8	-4.5	0.2	-2.1	1.5
Tenorite	$Cu(OH)_2.H_2O$	18	-7.3	-0.1	-5.3	1.9
Smithsonite	$ZnCO_3$	8	-6.1	-0.3	-4.0	1.8
Cerussite	$PbCO_3$	8	-5.9	-0.7	-3.5	1.6
Sphaerocobaltite	$CoCO_3$	8	-6.9	-2.6	-4.6	1.3
Theophrasite	$Ni(OH)_2$	18	-10.1	-3.4	-7.8	2.0
Eskolaite	Cr_2O_3	3	-11.3	-9.9	-10.6	0.7
Au metal	Au	18	-0.8	4.9	2.0	1.5
Iodyrite	AgI	3	-1.4	-0.7	-1.1	0.4
	$CaMoO_4$	1	-0.8	-0.8	-0.8	-
	$FeWO_4$	6	-6.0	-4.9	-5.4	0.4
	$Sb(OH)_3$	7	-0.9	-0.3	-0.7	0.2
Chervitite	$Pb_2V_2O_7$	1	-2.5	-2.5	-2.5	-
	YPO_4	17	-3.9	-0.1	-2.2	1.3
	$LaPO_4$	17	-4.4	0.2	-3.0	1.4
	$PrPO_4$	11	-4.6	-1.6	-3.6	1.1
	$SmPO_4$	18	-4.8	0.0	-2.9	1.5
	$YbPO_4$	8	-5.5	-4.2	-4.9	0.5

- standard deviation not calculated (single value)

The groundwaters at Carosue Dam have salinities well below that required for halite saturation (Figure A3.1), although the most saline samples are in equilibrium with gypsum (Figure A3.2). Disregarding the pH 7.1 sample, other major elements that appear to be controlled by equilibration with respect to a number of minerals in some or all of the groundwaters are Ba (barite; Figure A3.4), Si (amorphous silica; Figure A3.8) and Al (kaolinite, alunite, jurbanite and possibly amorphous alumina; Figures A3.10 - A3.13). Aluminium concentrations increase markedly below pH 5 (Figure A2.17) and Si also shows an increase in solubility with lower pH (Figure A2.18). This is presumably due to dissolution of alumino-silicates at the lower pH. Below pH 3.8, groundwaters are in equilibrium with kaolinite (Figure A3.10), indicating that even this normally resistant mineral can be dissolved under these conditions. At least some of the released Al is most probably incorporated into alunite, giving rise to the K depletion discussed above. However, the gross over-saturation of the groundwaters with respect to alunite (Figure A3.11), and the close equilibration with jurbanite across 3 pH units (Figure A3.12) suggests that Al is not DIRECTLY precipitating as alunite, but instead as an intermediate, possibly amorphous, Al-sulphate which then absorbs K and transforms to alunite. This is discussed in detail in Gray (1990).

The anomalous neutral groundwater in the SW of the study area markedly differs from other groundwaters in terms of major (and minor; Section 6.5) element equilibration. Major element solubility controls may include Ca (calcite; Figure A3.5), Mg (sepiolite, dolomite and/or magnesite; Figures A3.6, A3.7 and A3.9), Ba (barite; Figure A3.4), Si (sepiolite, commonly precipitated within valley calcretes; Mann and Horwitz, 1979; Figure A3.9) and Mn (rhodochrosite; Figure A3.15)

6.5 Minor element hydrogeochemistry

Concentrations of the minor elements (Table 5; Figures A2.19 - A2.46) show some similarities to Kalgoorlie groundwaters, as expected for an acid/saline environment (discussed in Gray, 1996). In particular, base metals and REE (*e.g.*, Figures A2.25 - A2.28, A2.39 and A2.40) have higher dissolved concentrations than the neutral central and northern groundwaters and have higher dissolved concentrations at lower pH, whereas anionic chalcophile elements (*e.g.*, As, Sb; Figures A2.31 and A2.38) have low concentrations. However, close examination of the data show some significant variations, which may be due to the different rock types to the other sites previously examined (*i.e.*, felsic rather than mafic/ultramafic). At Carosue Dam, Sc, Y, REE, Pb, U, Cr and, to a lesser extent, Mn, Co and Ni (Figures A2.19, A2.32, A2.39, A2.40, A2.43, A2.46, A2.22, A2.23, A2.25 and A2.26) tend to have significantly lower concentrations at any particular pH than those for the Kalgoorlie groundwaters (which are mainly associated with mafic/ultramafic lithologies). Thus, for example, dissolved Sc concentration is below detection in most Carosue Dam groundwaters, only being above detection below pH 3.4 (Figure 35). In contrast, high dissolved Sc concentrations are observed for mafic/ultramafic rocks in other regions of the Yilgarn. This lithological discrimination has been previously observed, in particular at Panglo where shales, mafic and ultramafic rocks all show distinct dissolved base metal signatures in groundwaters (Gray, 1990).

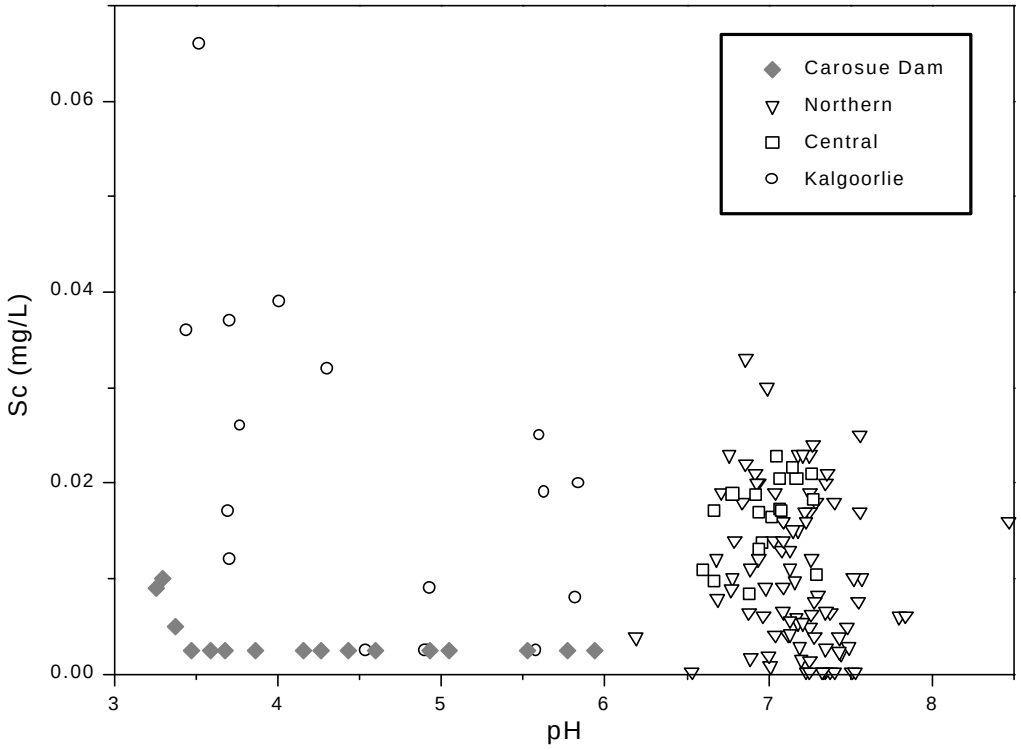

Figure 35: Scandium vs. pH for Carosue Dam and other Western Australian groundwaters.

Table 5: Median minor element compositions of groundwaters.

	Carosue Dam samples		Northern	Central	Kalgoor-lie	Mulga Rock	Sea water	Controls
	Acid (17)	pH 7.1 (1)						
I	2.0 ± 2.4	1.6	0.2	5	5.8	0.32	0.06	S/Sal ?
Li	0.22 ± 0.06	0.44	<0.005	<0.005	0.9	nd	0.18	Ac ?
Rb	0.070 ± 0.020	0.112	0.013	0.051	0.032	nd	0.12	Min ?
Ba	0.024 ± 0.008	0.044	0.04	0.02	0.04	0.03	0.013	Eq/Min
Sc	< 0.005	< 0.005	0.009	0.017	0.019	nd	0.0000006	Ac/Min
V	< 0.005	< 0.005	0.007	<0.005	<0.005	nd	0.002	?
Cr	< 0.005	< 0.005	0.01	<0.005	0.003	0.002	0.0003	Um
Mn	3.5 ± 2.4	5.3	0.01	0.1	2	0.3	0.0002	Mf/Um/Ac
Fe	0.17 ± 0.68	< 0.02	0.003	0.05	0.1	1	0.002	S
Co	0.15 ± 0.09	0.05	<0.0005	0.002	0.16	<0.002	0.00002	Um/Mf/Ac
Ni	0.25 ± 0.14	0.08	0.002	0.001	0.26	0.020	0.00056	Ac/Mf/Um
Cu	0.09 ± 0.07	1.27	0.003	0.003	0.05	0.00	0.00025	Ac/Mf
Zn	0.41 ± 0.23	43	0.006	0.01	0.05	0.04	0.0049	Ac/Mf
Ga	0.004 ± 0.002	0.016	0.002	<0.005	0.006	nd	0.00003	S
As	< 0.02	< 0.02	<0.0002	0.09	<0.02	<0.02	0.0037	S
Mo	0.005 ± 0.000	0.01	0.001	0.009	<0.01	nd	0.01	S
Ag	< 0.005	< 0.005	<0.001	0.0005	0.001	nd	0.00004	?
Cd	0.00 ± 0.00	0.01	<0.002	0.001	<0.002	<0.001	0.00011	?
Sb	< 0.001	0.003	<0.0003	0.001	<0.001	<0.0004	0.00024	S
REE	0.09 ± 0.60	< 0.001	<0.002	<0.008	0.8	0.013	0.000013	Ac
W	0.001 ± 0.001	0.007	<0.0002	0.001	0.001	nd	0.0001	S
Au	0.33 ± 0.84	0.014	0.004	0.03	0.05	0.001	0.004	Min
Hg	nd	nd	<0.0002	<0.001	0.002	<0.001	0.00003	S
Tl	0.002 ± 0.002	0.008	<0.0002	0.001	<0.002	0.0005	0.000019	S
Pb	0.031 ± 0.025	0.443	<0.001	0.001	0.06	0.012	0.00003	Ac/Min
Bi	< 0.001	< 0.001	<0.0002	0.001	<0.001	<0.002	0.00002	S ?
Th	< 0.001	0.001	<0.0002	<0.001	<0.002	<0.001	0.000001	?
U	0.002 ± 0.003	0.002	0.0003	0.002	0.004	<0.002	0.0032	Ac

All concentrations in mg/L (ppm), except Au in µg/L (ppb) nd: not determined
Number of samples given in brackets

Eq mineral equilibrium
Ac enriched in acid groundwaters
Um enriched in waters contacting ultramafic rocks
Mf enriched in waters contacting mafic rocks
Min enriched in waters contacting Au mineralization
S enriched in waters contacting weathering sulphides
Sal enriched in saline groundwaters
? not clearly defined

The concentrations of many minor elements are high for the Carosue Dam groundwaters, due to their low pH. However, as discussed above, at any particular pH, dissolved minor element concentrations at Carosue Dam are comparable, or less than, observed for other groundwaters in mineralized areas, with the possible exception of Au (Section 6.6). This suggests that groundwaters contacting weathered felsic rocks are likely to show reduced hydrogeochemical signatures, once pH effects are taken into account. This should be confirmed in other areas of felsic rocks, and particularly areas of more pervasive neutral and/or fresh groundwater conditions.

The single groundwater sample with neutral pH, discussed separately in Section 6.4, and listed separately in Table 5, shows highly distinctive minor element chemistry, being enriched in Mo, Sb, W, Tl, Th and particularly Ga, Pb (0.44 mg/L), Cu (1.3 mg/L) and Zn (43 mg/L) (Figures A2.27 - A2.29, A2.34, A2.36, A2.38, A2.41, A2.43 and A2.45), relative to the other Carosue Dam groundwaters. The modest enrichment in the anionic chalcophile elements (Mo, Sb, W and Tl) could be due to enhanced solubility

at neutral pH, compared with acid conditions, as discussed at the beginning of this Section. However, the Pb, Ga and, particularly, Cu and Zn concentrations are highly anomalous, the latter two being higher than that previously observed by this author in the Yilgarn Craton. Indeed, this groundwater is in equilibrium with secondary Mn, Cu, Zn and possibly Pb minerals (Figures A3.15 - A3.18), indicating high concentrations of these elements being released into the groundwater. The reason for this anomaly is not clear. Although the possibility of contamination should not be totally discounted, there is nothing in the sample characteristics or the area at the time of sampling to indicate this.

Therefore, the observed minor element enrichments in these groundwaters may well represent release from weathering minerals, and groundwater distributions (Appendix 4) may relate to lithological changes, or differing chemistry of mineralized zones.

6.6 Gold chemistry

The high salinity of the groundwaters at this site means that the dominant mechanism for the mobilization of Au in the southern Yilgarn, namely as the chloride complex ($AuCl_2^-$):

$$2Au_{(S)} + 4Cl^- + O_2 + 2H^+ \Leftrightarrow 2AuCl_2^- + H_2O \quad ...(1)$$

is expected to be significant for the shallow groundwaters at Carosue Dam, though less important for deeper, more reduced groundwaters. Both acid and oxidising conditions are also required for Au dissolution, as is observed at this site (Figure 33). As expected, Au concentrations are, unlike other minor elements, as high if not higher than for other Yilgarn sites (Figure 36). Speciation analysis also indicates that the iodide complex AuI_2^- may also be important, which is why the calculated Eh levels for Au dissolution (Figure 33) are lower than reported elsewhere. Most Carosue groundwaters are either at or slightly above equilibrium for Au metal, particularly below pH 3.8 (Figure A3.25).

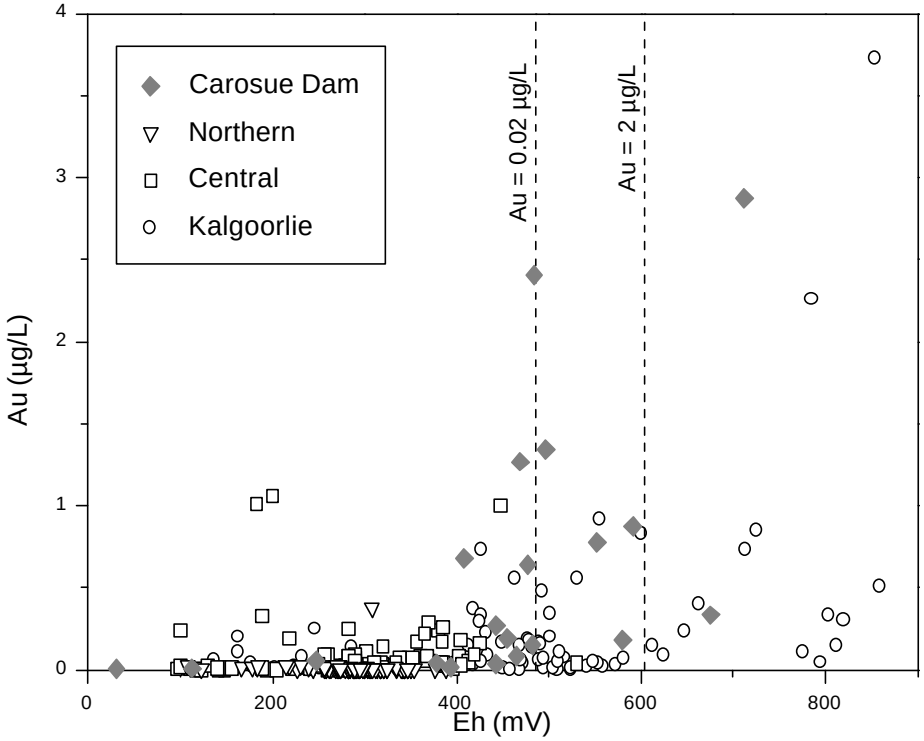

Figure 36: Dissolved Au concentration vs. Eh for Carosue Dam and other Western Australian groundwaters, with the Eh values for dissolution of 0.02 and 0.2 µg/L Au.

6.7 Mapping of the groundwater data

Element distributions of Carosue Dam groundwaters are given in Appendix 4, Figures A4.1 - A4.30. Because of the strong pH and salinity control of many elements and the low concentrations of anionic

chalcophile elements (see above), very few elements give useful hydrogeochemical signatures. This is commonly observed for acid groundwaters (Gray, 1996). Additionally, many elements show particular enrichments for the previously discussed anomalous sample in the SW of the study area. As expected, the best (though still patchy) correlation with mineralization was for dissolved Au concentration (Figure 37). A clearly correlation may well have been observed if more background samples were available.

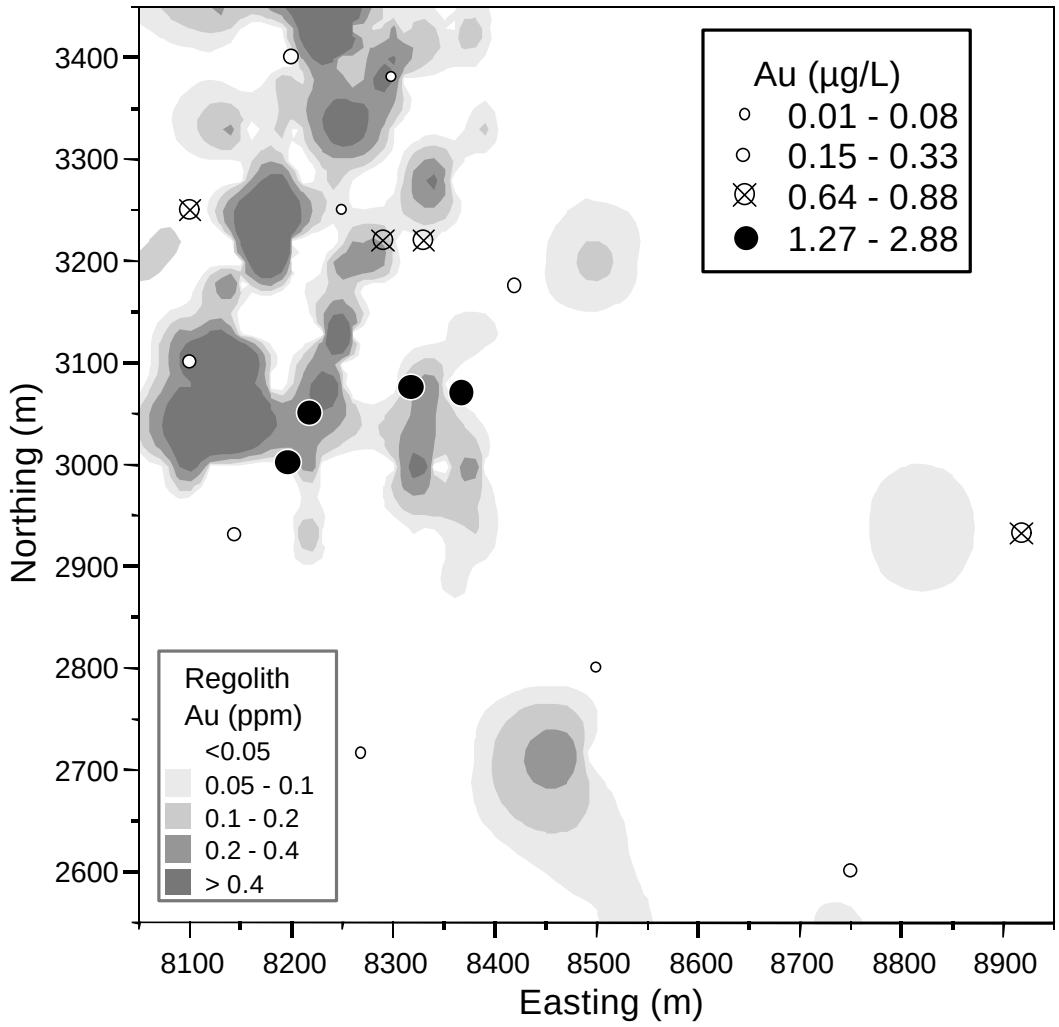

Figure 37: Dissolved Au distribution at Carosue Dam, with calculated Au distribution for 314 - 331 mRL shown as solid fill.

7. SUMMARY AND CONCLUSIONS

Carosue Dam differs from most other sites studied by CSIRO / CRC LEME in that Au mineralisation occurs in felsic rocks (volcanoclastic sandstones and trachyte volcanics). The whole area is generally flat and deeply weathered, with a surface layer (generally 1 - 6 m) of carbonate, within 5 - 20 m colluvium-alluvium, lacustrine clays and quartz sands. The *in situ* regolith is composed of 0 - 30 m of ferruginous material, generally truncated to mottled zone and 10 - 96 m of saprolite designated as strongly, moderately or weakly oxidised. The saprolite is strongly depleted in Au to 330 m RL (*i.e.*, approximately 30 m below surface, approximating to the base of the strongly oxidised zone), *i.e.*, the strongly oxidised zone, ferruginous zone and the transported cover (though not the carbonate zone) are all Au-poor. There is little indication of Au dispersion during initial weathering.

There is a clear Au enrichment at surface, associated with calcrete, apparently translocated several hundred metres south and upslope, relative to the underlying mineralization. The northern part of the mineralization has strongly truncated laterite and a thick transported zone and therefore reduced Au transport to the surface. The central part of the mineralization is the only part of the study area with conditions conducive to a Au anomaly at the surface, with mineralization, moderately intact residuum and less than 10 m of transported cover. The surface Au distribution is statistically less skewed than at depth, indicating significant redistribution. However, gold grain studies demonstrating a significant primary component to this Au indicate that a large part of this surface mobility is physical transport of primary Au, presumably transported southwards.

The Carosue Dam groundwaters are saline to hypersaline (2.5 - 11.6% TDS), and generally acid (pH 3.2 - 6.0), similar to Kalgoorlie groundwaters, though 2 - 3 times less saline. The Carosue Dam groundwaters show significant K depletion, probably due to alunite precipitation under acid conditions. Concentrations of the minor elements show some similarities to the acid and saline Kalgoorlie groundwaters. In particular, base metals and REE have greater dissolved concentrations than the neutral central and northern groundwaters, whereas anionic chalcophile elements (*e.g.*, As, Sb) have low concentrations. However, at Carosue Dam, Sc, Y, REE, Pb, U, Cr and, to a lesser extent, Mn, Co and Ni tend to have significantly lower concentrations at any pH than those for the Kalgoorlie groundwaters (representing primarily mafic and ultramafic lithologies) and show very strong pH control on the solubility. This suggests that groundwaters contacting weathered felsic rocks are likely to show reduced hydrogeochemical signatures, once pH effects are taken into account.

The high salinity and acidity of the shallow groundwaters at this site means that the dominant mechanisms for the mobilization of Au, typical of the southern Yilgarn, would be the chloride ($AuCl_2^-$) or iodide (AuI_2^-) complexes, though this would be less important for deeper, more reduced groundwaters. The groundwaters range from moderately to highly oxidising: two of the groundwaters have Eh values high enough to allow dissolution of > 2 µg/L Au, with another three groundwaters able to dissolve > 0.2 µg/L Au. As a consequence, Au concentrations are, unlike other minor elements, as high if not higher than other Yilgarn sites. Because of the strong control by salinity and acidity, very few elements give useful hydrogeochemical signatures for exploration. The best (though patchy) correlation with mineralization was for dissolved Au.

ACKNOWLEDGEMENTS

We would like to thank Aberfoyle Resources Ltd, who provided access to the Carosue Dam site and to their exploration database. Personnel including Michael Joyce and Hugh Rowlands are greatly acknowledged for their support. Additional access to the later drilling database was provided by Pacmin Mining Corporation. We also received laboratory support from Dale Longman and Michael Hart at CSIRO, Perth and from Lesley Dotter at CSIRO, Sydney. Dr Charles Butt provided advice during the preparation of this report.

REFERENCES

Bristow, A.P.J., Lintern M.J. and Butt, C.R.M., 1996b. Geochemical expression of concealed gold mineralisation, Safari Prospect, Mt Celia, Western Australia. CSIRO Division of Exploration and Mining Restricted Report 281R, Perth, Australia. 58 pp.

Bristow, A.P.J., Gray, D.J. and Butt, C.R.M., 1996a. Geochemical and spatial characteristics of regolith and groundwater around the Golden Delicious Prospect, Western Australia. CSIRO Division of Exploration and Mining Restricted Report 280R, Perth, Australia. 175 pp.

Butt, C.R.M., Gray, D.J., Robertson, I.D.M., Lintern, M.J., Anand, R.R., Britt, A., Bristow, A.P.J., Munday, T.J., Phang, C., Smith, R.E. and Wildman, J.E., 1997. AMIRA P409 - Yilgarn Transported Overburden Final Report. CSIRO Division of Exploration and Mining Restricted Report 333R, Perth, Australia. 164 pp.

Douglas, G.B., Gray, D.J. and Butt, C.R.M., 1993. Geochemistry, Mineralogy and Hydrogeochemistry of the Ambassador Multi Element Lignite Deposit, Western Australia. CSIRO Division of Exploration Geoscience Restricted Report 337R, Perth, Australia.

Drever, J.I., 1982. "The Geochemistry of Natural Waters." Prentice-Hall, Inc., Englewood Cliffs, N.J. U.S.A. 388 p.

Gray, D.J., 1990. Hydrogeochemistry of the Panglo Gold Deposit. CSIRO Division of Exploration Geoscience Restricted Report 125R, Perth, Australia. 74 pp.

Gray, D.J., 1991. Hydrogeochemistry in the Mount Gibson Gold District. CSIRO Division of Exploration Geoscience Restricted Report 120R, Perth, Australia. 80 pp.

Gray, D.J., 1992a. Hydrogeochemistry of Sulphide Weathering at Boags Pit, Bottle Creek, Western Australia. CSIRO Division of Exploration Geoscience Restricted Report 237R, Perth, Australia. 13 pp.

Gray, D.J., 1992b. Geochemical and Hydrogeochemical Investigations of Alluvium at Mulgarrie, Western Australia. CSIRO Division of Exploration Geoscience Restricted Report 339R, Perth, Australia. 66 pp.

Gray, D.J., 1993a. Investigation of the Hydrogeochemical Dispersion of Gold and other Elements from Mineralized Zones at the Granny Smith Gold Deposit, Western Australia. CSIRO Division of Exploration Geoscience Restricted Report 383R, Perth, Australia. Volumes I and II. 93 pp.

Gray, D.J., 1993b. Investigation of the Hydrogeochemical Dispersion of Gold and other Elements in the Wollubar Palaeodrainage, Western Australia. CSIRO Division of Exploration Geoscience Restricted Report 387R, Perth, Australia. Volumes I and II. 133 pp.

Gray, D.J., 1994. Investigation of the Hydrogeochemical Dispersion of Gold and other Elements at Lawlers, Western Australia. CSIRO Division of Exploration and Mining Restricted Report 26R, Perth, Australia. Volumes I and II. 151 pp.

Gray, D.J., 1995. Hydrogeochemical Dispersion of Gold and other Elements at Baxter, Western Australia. CSIRO Division of Exploration and Mining Restricted Report 169R, Perth, Australia. 85 pp.

Gray, D.J., 1996. Hydrogeochemistry in the Yilgarn Craton. CSIRO Division of Exploration and Mining Restricted Report 312R, Perth, Australia. 75 pp.

Lintern, M.J., and Gray, D.J., 1995a. Progress Statement for the Kalgoorlie Study Area - Steinway Prospect, Western Australia. CSIRO Division of Exploration and Mining Restricted Report No. 95R, Perth, Australia. 121 pp.

Lintern, M.J., and Gray, D.J., 1995b. Progress Statement for the Kalgoorlie Study Area - Argo Deposit, Western Australia. CSIRO Division of Exploration and Mining Restricted Report No. 96R, Perth, Australia. 153 pp.

Mann, A.W. and Horwitz, R.C., 1979. Groundwater calcrete deposits in Australia: some observations from Western Australia. Journal of Geological Society of Australia, 26: 293-303.

Murphy, J. and Riley, J.P., 1962. A modified single solution method for the determination of phosphate in natural waters. Analytica Chimica Acta, 27: 31-36.

Parkhurst, D.L., Thorstenson, D.C. and Plummer, L.N., 1980. PHREEQE, a computer program for geochemical calculations. U.S. Geological Survey Water Resources Investigations 80-96, 210p.

Plummer, L.N., and Parkhurst, D.L., 1990, Application of the Pitzer Equations to the PHREEQE geochemical model, in D.C. Melchior and R.L. Bassett (Editors), Chemical modeling of aqueous systems II: American Chemical Society Symposium Series 416, Washington, D.C., American Chemical Society, p. 128-137.

Weast, R.C., 1983. CRC Handbook of Chemistry and Physics, 63rd Edition. CRC Press, Inc., Boca Raton, Florida.

Zall, D.M., Fisher, D. and Garner, M.D., 1956. Photometric determination of chlorides in water. Analytical Chemistry, 28:1665.

APPENDICES

APPENDIX 1: CONTENTS OF ENCLOSED CD

A1. CAROSUE PICTURE DATABASE

The Carosue Dam Picture database is included as BMP files in separate directories on the accompanying CD, as described briefly, and then listed below.

A1.1 Directory description

(i) the SliceN directory includes vertical slices at constant northing, with plots named according to the particular northing;

(ii) the SliceE directory includes vertical slices at constant easting, with plots named according to the particular easting. Thus the plot shown in Figure 30 is named 8200mE.bmp;

(iii) the Cut-offs directory includes the various layers coloured as in Figure 5, either merged together to show the true stratigraphy (Layers.bmp), exploded as in Figure 5 so as to show the characteristics of the various layers (Exp_Au.bmp), or with a particular Au grade cut-off (thus the plot shown in Figure 29 is named 50ppbAu.bmp);

(iv) the Plans directory includes plans of regolith distribution or calculated Au grade at a particular RL (*e.g.*, the plot of the calculated Au concentrations at 300 mRL is named 300mRL-Au.bmp) at a particular surface (*e.g.*, the plot of the calculated Au grade at the unconformity is named Unconf-Au.bmp) or at a set vertical distance from a weathering surface (*e.g.*, the plot of the calculated Au grade 2 m below base of weathering the is named bow-2-Au.bmp).

(v) the Interactive directory includes interactive 3D models written with Virtual Reality Modelling Language (VRML) which can be manipulated by the user (rotate, pan, zoom) and simply require an internet browser (Netscape, Explorer, no outside line necessary) with a plug-in that is provided on the CD.

A1.2 List of files

A1.2.1 Slice N directory

2700mN.bmp - Calculated Au distribution for 2700 mN East/RL slice
2750mN.bmp - Calculated Au distribution for 2750 mN East/RL slice
2800mN.bmp - Calculated Au distribution for 2800 mN East/RL slice
2850mN.bmp - Calculated Au distribution for 2850 mN East/RL slice
2900mN.bmp - Calculated Au distribution for 2900 mN East/RL slice
2950mN.bmp - Calculated Au distribution for 2950 mN East/RL slice
3000mN.bmp - Calculated Au distribution for 3000 mN East/RL slice
3050mN.bmp - Calculated Au distribution for 3050 mN East/RL slice
3075mN.bmp - Calculated Au distribution for 3075 mN East/RL slice
3100mN.bmp - Calculated Au distribution for 3100 mN East/RL slice
3150mN.bmp - Calculated Au distribution for 3150 mN East/RL slice
3200mN.bmp - Calculated Au distribution for 3200 mN East/RL slice
3250mN.bmp - Calculated Au distribution for 3250 mN East/RL slice
3300mN.bmp - Calculated Au distribution for 3300 mN East/RL slice
3350mN.bmp - Calculated Au distribution for 3350 mN East/RL slice
3400mN.bmp - Calculated Au distribution for 3400 mN East/RL slice
3450mN.bmp - Calculated Au distribution for 3450 mN East/RL slice
3500mN.bmp - Calculated Au distribution for 3500 mN East/RL slice
3550mN.bmp - Calculated Au distribution for 3550 mN East/RL slice

A1.2.2 Slice E directory

8050mE.bmp - Calculated Au distribution for 8050 mE North/RL slice
8100mE.bmp - Calculated Au distribution for 8100 mE North/RL slice
8150mE.bmp - Calculated Au distribution for 8150 mE North/RL slice
8200mE.bmp - Calculated Au distribution for 8200 mE North/RL slice
8250mE.bmp - Calculated Au distribution for 8250 mE North/RL slice
8300mE.bmp - Calculated Au distribution for 8300 mE North/RL slice

8350mE.bmp - Calculated Au distribution for 8350 mE North/RL slice
8400mE.bmp - Calculated Au distribution for 8400 mE North/RL slice
8450mE.bmp - Calculated Au distribution for 8450 mE North/RL slice

A1.2.3 Cut-offs directory

Exp_Layers.bmp- Regolith stratigraphic layers exploded so as to show the characteristics of the various layers
Layers.bmp - Regolith stratigraphic layers merged together to show the true stratigraphy
Au_Layers.bmp - Au distribution on merged regolith stratigraphic layers.
Exp_Au.bmp - Au distribution on exploded regolith stratigraphic layers.
BAse_calcrete.bmp - Au distribution below the base of calcrete.
20ppbAu.bmp - Regolith stratigraphic layers merged together, with a 0.02 ppm Au grade cut-off
50ppbAu.bmp - Regolith stratigraphic layers merged together, with a 0.05 ppm Au grade cut-off
100ppbAu.bmp - Regolith stratigraphic layers merged together, with a 0.1 ppm Au grade cut-off
200ppbAu.bmp - Regolith stratigraphic layers merged together, with a 0.2 ppm Au grade cut-off
500ppbAu.bmp - Regolith stratigraphic layers merged together, with a 0.5 ppm Au grade cut-off
1ppmAu.bmp - Regolith stratigraphic layers merged together, with a 1 ppm Au grade cut-off
2ppmAu.bmp - Regolith stratigraphic layers merged together, with a 2 ppm Au grade cut-off

A1.2.4 Plans directory

220mRL-Au.bmp - Calculated Au distribution at 220 mRL
230mRL-Au.bmp - Calculated Au distribution at 230 mRL
230mRL-Reg.bmp - Regolith distribution at 230 mRL
240mRL-Au.bmp - Calculated Au distribution at 240 mRL
240mRL-Reg.bmp - Regolith distribution at 240 mRL
250mRL-Au.bmp - Calculated Au distribution at 250 mRL
250mRL-Reg.bmp - Regolith distribution at 250 mRL
260mRL-Au.bmp - Calculated Au distribution at 260 mRL
260mRL-Reg.bmp - Regolith distribution at 260 mRL
270mRL-Au.bmp - Calculated Au distribution at 270 mRL
270mRL-Reg.bmp - Regolith distribution at 270 mRL
280mRL-Au.bmp - Calculated Au distribution at 280 mRL
280mRL-Reg.bmp - Regolith distribution at 280 mRL
290mRL-Au.bmp - Calculated Au distribution at 290 mRL
290mRL-Reg.bmp - Regolith distribution at 290 mRL
300mRL-Au.bmp - Calculated Au distribution at 300 mRL
300mRL-Reg.bmp - Regolith distribution at 300 mRL
310mRL-Au.bmp - Calculated Au distribution at 310 mRL
310mRL-Reg.bmp - Regolith distribution at 310 mRL
320mRL-Au.bmp - Calculated Au distribution at 320 mRL
320mRL-Reg.bmp - Regolith distribution at 320 mRL
330mRL-Au.bmp - Calculated Au distribution at 330 mRL
330mRL-Reg.bmp - Regolith distribution at 330 mRL
340mRL-Au.bmp - Calculated Au distribution at 340 mRL
340mRL-Reg.bmp - Regolith distribution at 340 mRL
350mRL-Au.bmp - Calculated Au distribution at 350 mRL
350mRL-Reg.bmp - Regolith distribution at 350 mRL
355mRL-Au.bmp - Calculated Au distribution at 355 mRL
355mRL-Reg.bmp - Regolith distribution at 355 mRL
360mRL-Au.bmp - Calculated Au distribution at 360 mRL
360mRL-Reg.bmp - Regolith distribution at 360 mRL
362mRL-Au.bmp - Calculated Au distribution at 362 mRL

362mRL-Reg.bmp - Regolith distribution at 362 mRL
Surface-Au.bmp - Calculated Au distribution at surface
base-calcrete-Au.bmp - Calculated Au distribution at the base of the calcrete
Unconf-Au.bmp - Calculated Au distribution at the unconformity
Base_ferr-Au.bmp - Calculated Au distribution at the base of the ferruginous material.(pedoplasmation front)
Str-mod-Au.bmp - Calculated Au distribution at the boundary between moderately and strongly weathered saprolite
Str-mod+2-Au.bmp - Calculated Au distribution 2 m above the boundary between moderately and strongly weathered saprolite
Str-mod+5-Au.bmp - Calculated Au distribution 5 m above the boundary between moderately and strongly weathered saprolite
Str-mod+10-Au.bmp - Calculated Au distribution 10 m above the boundary between moderately and strongly weathered saprolite
Str-mod-2-Au.bmp - Calculated Au distribution 2 m below the boundary between moderately and strongly weathered saprolite
Str-mod-5-Au.bmp - Calculated Au distribution 5 m below the boundary between moderately and strongly weathered saprolite
Str-mod-10-Au.bmp - Calculated Au distribution 10 m below the boundary between moderately and strongly weathered saprolite
Mod-weak-Au.bmp - Calculated Au distribution at the boundary between weakly and moderately weathered saprolite
Mod-weak+2-Au.bmp- Calculated Au distribution 2 m above the boundary between weakly and moderately weathered saprolite
Mod-weak+5-Au.bmp- Calculated Au distribution 5 m above the boundary between weakly and moderately weathered saprolite
Mod-weak+10-Au.bmp- Calculated Au distribution 10 m above the boundary between weakly and moderately weathered saprolite
Mod-weak-2-Au.bmp - Calculated Au distribution 2 m below the boundary between weakly and moderately weathered saprolite
Mod-weak-5-Au.bmp - Calculated Au distribution 5 m below the boundary between weakly and moderately weathered saprolite
Mod-weak-10-Au.bmp - Calculated Au distribution 10 m below the boundary between weakly and moderately weathered saprolite
bow-Au.bmp - Calculated Au distribution at the base of weathering
bow+2-Au.bmp - Calculated Au distribution 2 m above the base of weathering
bow+5-Au.bmp - Calculated Au distribution 5 m above the base of weathering
bow+10-Au.bmp - Calculated Au distribution 10 m above the base of weathering
bow-2-Au.bmp - Calculated Au distribution 2 m below the base of weathering
bow-5-Au.bmp - Calculated Au distribution 5 m below the base of weathering
bow-10-Au.bmp - Calculated Au distribution 10 m below the base of weathering
bow-20-Au.bmp - Calculated Au distribution 20 m below the base of weathering
bow-40-Au.bmp - Calculated Au distribution 40 m below the base of weathering

A1.2.5 Interactive directory

The enclosed CD contains a folder called “interactive”. It consists of:

- A web page – “Carosue.htm” and an associated “images” folder.
- A folder called “vrmls” which contains VRMLs (files written with Virtual Reality Modelling Language). These are 3D images that the user can manipulate and view from different angles.
- An installation file for Cosmo Player.

You will need to have a web browser installed on your computer (but it does not have to be connected to an outside line). You will need a plug-in, such as COSMO Player, that will enable your internet browser to display the VRMLs. To install Cosmo Player from this CD, follow the steps below (which are also set out on the web page).

Note: The computer will need at least 200 Mhz and 64 MB to run the VRMLs effectively.

Instructions for viewing VRMLs

1. Open the CD, then open the "interactive" folder. Click on the icon named "cosmo_win95nt_eng.exe" and it will launch with prompts. Read the first page, close any open Windows programs, then click NEXT.
2. Agree to the License Agreement and click YES.
3. It will determine which internet browsers are on your system and list some options. Choose the option that you usually use, e.g. Netscape Communicator 4.5 or Internet Explorer (provided with Windows). Some users will have older systems and will need to choose "Other". Click NEXT.
4. Choose the destination folder using the BROWSE button. Then click NEXT. The plug-in will now install itself.
5. It will then ask you if you would like to associate all VRML related files (.wrl, .wrz, .wrl.gz) with Cosmo Player. Choose YES.
6. Set up is complete. You should be able click on the options below and use the VRMLs.

Web Page

A web page is provided as a convenient way of navigating through the VRMLs. In particular, it provides a handy reference to the regolith legend as this feature is not supported by the VRMLs.

Either open the page through your browser (File Menu – Open Page) or if your computer is configured to recognise htm/html files then just click on the "Carosue.htm" icon to launch the page.

The following VRMLs are provided:

Carosue Dam 3D Au Cut-offs

These VRMLs depict three-dimensional models of Au distribution at the Carosue Dam deposit. The colours match the regolith legend and show all those parts of each regolith layer that have, for example, 300 ppb Au concentration or greater.

File:	**Depicts:**
50ppb.wrl	Au distribution with 50 ppb cut-off
100ppb.wrl	Au distribution with 100 ppb cut-off
200ppb.wrl	Au distribution with 200 ppb cut-off
500ppb.wrl	Au distribution with 500 ppb cut-off
1ppm.wrl	Au distribution with 1 ppm cut-off

APPENDIX 2: ELEMENT/ION CONCENTRATIONS FOR GROUNDWATERS

APPENDIX 3: SATURATION INDICES FOR GROUNDWATERS

APPENDIX 4: ELEMENT/ION DISTRIBUTION MAPS FOR GROUNDWATERS